Atmospheric Research 137 (2014) 145–166

Contents lists available at ScienceDirect

Atmospheric Research

journal homepage: www.elsevier.com/locate/atmos

Uncertainty analysis of bias from satellite rainfall estimates using copula method

Saber Moazami [a,d,*], Saeed Golian [b], M. Reza Kavianpour [a], Yang Hong [c,d]

[a] School of Civil Engineering, K.N. Toosi University of Technology, 470 Mirdamad Ave. West, 19697, Tehran 19697 64499, Iran
[b] Civil Engineering Department, Shahrood Univerity of Technology, Shahrood 36199 95161, Iran
[c] School of Civil Engineering and Environmental Sciences, University of Oklahoma, Norman, OK 73072, USA
[d] Advanced Radar Research Center, University of Oklahoma, 120 David L. Boren Blvd., Suite 4610, Norman, OK 73072, USA

ARTICLE INFO

Article history:
Received 20 December 2012
Received in revised form 16 August 2013
Accepted 20 August 2013
Available online 30 September 2013

Keywords:
Satellite rainfall estimates
PERSIANN
TMPA-3B42
Bias-adjustment
Copula
Uncertainty

ABSTRACT

The aim of this study is to develop a copula-based ensemble simulation method for analyzing the uncertainty and adjusting the bias of two high resolution satellite precipitation products (PERSIANN and TMPA-3B42). First, a set of sixty daily rainfall events that each of them occurs concurrently over twenty 0.25° × 0.25° pixels (corresponding to both PERSIANN and TMPA spatial resolution) is determined to perform the simulations and validations. Next, for a number of fifty-four out of sixty (90%) selected events, the differences between rain gauge measurements as reference surface rainfall data and satellite rainfall estimates (SREs) are considered and termed as observed biases. Then, a multivariate Gaussian copula constructed from the multivariate normal distribution is fitted to the observed biases. Afterward, the copula is employed to generate multiple bias fields randomly based on the observed biases. In fact, copula is invariant to monotonic transformations of random variables and thus the generated bias fields have the same spatial dependence structure as that of the observed biases. Finally, the simulated biases are imposed over the original satellite rainfall estimates in order to obtain an ensemble of bias-adjusted rainfall realizations of satellite estimates. The study area selected for the implementation of the proposed methodology is a region in the southwestern part of Iran. The reliability and performance of the developed model in regard to bias correction of SREs are examined for a number of six out of those sixty (10%) daily rainfall events. Note that these six selected events have not participated in the steps of bias generation. In addition, three statistical indices including bias, root mean square error (RMSE), and correlation coefficient (CC) are used to evaluate the model. The results indicate that RMSE is improved by 35.42% and 36.66%, CC by 17.24% and 14.89%, and bias by 88.41% and 64.10% for bias-adjusted PERSIANN and TMPA-3B42 estimates, respectively.

1. Introduction

High resolution satellite rainfall estimates (SREs) provide a useful source of data (i.e. uninterrupted and global coverage) for hydrological applications and water resources planning, particularly over developing regions in which ground-based observations are usually sparse or unevenly distributed. However, using satellite products is subject to error and uncertainty due to the indirect nature of their estimates. On the other hand, reliable estimation of precipitation is essential for hydrologists, as the uncertainties associated with rainfall estimates will propagate in hydrologic modeling predictions (Aghakouchak, 2010). Therefore, in this study, the authors focus on the bias simulation and adjustment of two widely used high resolution satellite products (PERSIANN and TMPA-3B42) over a region in the southwest of Iran.

* Corresponding author at: National Weather Center, Advanced Radar Research Center, Suite 4636, 120 David L. Boren Blvd., Norman, OK 73072-7303, USA. Tel.: +1 404 858 1991.
E-mail addresses: saber.moazami@ou.edu, saber.moazami@gmail.com (S. Moazami).

0169-8095/$ – see front matter © 2013 Elsevier B.V. All rights reserved.
http://dx.doi.org/10.1016/j.atmosres.2013.08.016

The evaluation of the accuracy of SREs has been carried out at different spatial and temporal resolutions in several studies in the last years (Tian et al., 2007; Hong et al., 2007; Su et al., 2008; Li et al., 2009; AghaKouchak et al., 2009, 2012; Hirpa et al., 2010; Dinku et al., 2010; Behrangi et al., 2011; Bitew and Gebremichael, 2011; Yong et al., 2012). However, the applicability of SREs in hydrologic predictions and water resources management is limited, due to a lack of quantitative information regarding the uncertainties of satellite precipitation estimates at required spatial and temporal resolution (Sorooshian et al., 2000).

One way to assess spatio-temporal uncertainties of satellite precipitation products is to simulate an ensemble of precipitation fields which consists of a large number of realizations; each realization represents a possible rainfall event (Aghakouchak, 2010). Hossain and Anagnostou (2006) developed a two-dimensional satellite rainfall error model (SREM2D) for simulating ensembles of satellite rain fields. They characterized the joint spatial probability of successful delineation of rainy and non-rainy areas using Bernoulli trials of the uniform distribution with a correlated structure generated based on Gaussian random fields. They also generated random error fields of SREs by Monte Carlo simulation of given realizations. Bellerby and Sun (2005) proposed a methodology to quantify the uncertainty present in high-resolution satellite precipitation estimates by generating probabilistic and ensemble representations of the measured precipitation field. Teo and Grimes (2007) described an approach for estimating the uncertainty on satellite-based rainfall values using ensemble generation of rainfall fields based on the stochastic calibration. They obtained the correct spatial correlation structure within each ensemble member by the use of geostatistical sequential simulation. Hong et al. (2006a,b) developed an uncertainty analysis framework to quantify PERSIANN-CCS precipitation estimates error characteristics into a range of discrete temporal (1, 3, 6, 12, and 24 h) and spatial (0.04°, 0.12°, 0.24°, 0.48°, and 0.96°) scales. They also generated ensemble members of precipitation data as forcing input to a conceptual rainfall-runoff hydrologic model using Monte Carlo simulation to examine the influence of precipitation estimation error on the uncertainty of hydrological response.

Note that in the aforementioned studies, the geostatistical approaches and Monte Carlo simulation were used to generate spatially correlated random fields and ensemble members of precipitation estimation error. Compared with a single best estimate, such ensemble-based models can provide more accurate quantification of precipitation uncertainty; however, geostatistical based methods (e.g. a simple variogram model or a covariance matrix) have some limitations. For example in data analysis by geostatistical models, the data should have three features including dependency, stationarity, and Gaussian distribution (Johnston, 2004). Also, in models like geostatistical sequential simulation which uses classical families of multivariate distributions such as bivariate normal, log-normal and gamma, dependence structure between variables is not independent on the choice of the marginal distributions (Genest and Favre, 2007). Therefore, using such models may lead to unrealistic simulations (Germann et al., 2006). Therefore, as an alternative approach, copulas that are joint cumulative distribution functions can be employed to describe the dependence structure of variables as well as to model multivariate random variables with different marginal distributions. In fact, describing the dependence structure independent of the marginal distribution is one of the most attractive features of copulas (Joe, 1997; Nelsen, 2006; Aghakouchak, 2010).

In recent years, several studies in regard to applications of different families of copula in hydrological and meteorological processes have been reported by Grimaldi and Serinaldi (2006), Renard and Lang (2007), Zhang and Singh (2007), Evin and Favre (2008), Serinaldi (2009a,b), Wang et al. (2010), Aghakouchak et al. (2010a,b,c), and Vandenberghe et al. (2010). In this study, we assess the uncertainty and adjust the bias of PERSIANN and TMPA-3B42 products using a copula-based ensemble generation method. For this reason, a multivariate Gaussian copula is employed to describe the dependence structure and to simulate multivariate satellite rainfall bias fields based on the observed biases of daily rainfall events over twenty 0.25° × 0.25° pixels. It is pointed out that the daily resolution of SREs is used in this paper because the reference rain gauge data are based on the daily measurements. Indeed, there doesn't exist a reliable set of sub-daily ground data across the study area.

The approach presented here is similar to that of Aghakouchak et al. (2010a,b,c) since it makes use of copula technique to generate an ensemble of rainfall realizations. However, in the proposed model by Aghakouchak et al. (2010a,b,c), the intention was to use copula-based simulation of multivariate error fields for radar rainfall estimates in order to generate an ensemble of rainfall realizations, while the aim of this study is to develop a bias correction model for satellite precipitation estimates. For this purpose, multiple bias fields are generated based on the observed biases of fifty-four daily rainfall events over twenty 0.25° × 0.25° pixels. Then, the generated biases are imposed over the original SREs in order to simulate an ensemble of bias-adjusted rainfall realizations of satellite estimates. To examine the reliability and performance of the developed model, the generated biases are also imposed over the six daily rainfall events which have not been involved in the steps of bias simulation. It is noted that these six selected events have occurred over the same pixels as those fifty-four events. In addition, the model presented here uses an uncertainty analysis technique (see Section 3.5) to select a more accurate set of biases among the several randomly generated sets which would result in better estimates.

It is worth pointing out that the 3B42 version of TMPA products presents the bias reduction data of precipitation estimates using the gauge data based on the Global Precipitation Climatology Project (GPCP) monthly rain gauge analysis (Rudolf, 1993). The gauge adjustment process involves aggregating both the gauge and the 3-hourly 3B42 estimates to a monthly scale and then applying the ratio of the 3B42/gauge monthly totals to each 3-hourly time step (Habib et al., 2009). However, several studies have reported the uncertainty associated with the TMPA-3B42 product over different regions (Jiang et al., 2012; AghaKouchak et al., 2009, 2011; Habib et al., 2009; Yong et al., 2012). Compared with TMPA-3B42 algorithm that assumes the precipitation estimation error as a fixed ratio of rain rates, the framework proposed based on the simulated ensembles of SREs bias fields provides more realistic quantification of uncertainties associated with different kinds of satellite precipitation products (Hong et al., 2006a,b).

The present work is organized as follows: Section 2 introduces the study area and data resources used; Section 3 describes the suggested methodology for adjusting the bias of SREs; Section 4 details the results and discussion; and Section 5 presents the conclusions and recommendations.

2. Study area and data resources

2.1. Study area

Khuzestan Province (30°–33° latitude, 47.7°–50.5° longitude) is one of the 31 provinces of Iran in the southwestern part of country with a total area of 63,238 km^2 (Fig. 1). Khuzestan contains more than 30% of the total surface water resources of the country, due to several prominent rivers (Karun, Karkheh, Dez, Jarahi and Arvand Rud) which flow over the entire territory of this province. On the other hand, the geography of Khuzestan encompasses terrain ranging from plains in the southern to mountains in the northern parts of the province. The northern parts covered by Zagros Mountains have temperate weather in the summer and cold weather in the winter season. The type of precipitation in this area with mountainous climate is orographic and the mean annual precipitation is around 700 mm. However, in the southern parts close to the Persian Gulf with mid-latitude, as well as tropical humid climate, most precipitation appears to be convective. Also, in this area with warm weather, the mean annual rainfall is less than 250 mm. The central parts of Khuzestan with semiarid climate are covered by steppe. Over this area the average value of rainfall has been reported in the range between 250 to 400 mm. In general, because of climate conditions governing in Khuzestan, there are long-duration and intense precipitation events across this region. Furthermore, overflowing great rivers after incessant heavy rain leads to major floods over the Khuzestan. Therefore, high resolution spatiotemporal information of rainfall as the most important input variable into hydrologic models is essential in order to simulate and analyze extreme events reliably. However, the availability of a dense network of ground-based rainfall measurements is relatively limited across the Khuzestan province. Then, as a possible alternative, high resolution satellite precipitation products can be employed in this area.

Khuzestan consists of around one hundred 0.25° × 0.25° pixels (corresponding to those PERSIANN and TMPA pixels); as well as there are eighty rain gauges across this region. To determine the appropriate pixels for this study, at the first step, forty pixels out of one hundred that each of them contains at least one rain gauge are determined. Then, a set of twenty pixels out of forty with the largest number of reference ground data associated with the daily rainfall events during the study period (2003–2006) is selected (Fig. 1*c*). It is noted that to perform the simulation and validation fields, a number of sixty daily rainfall events are selected, each of which is concurrent over all the twenty pixels. Consequently, the analyses are implemented for the sixty daily events over the twenty pixels in the study area.

2.2. Data resources

The true reference data set employed in the present work is based on the daily rain gauge observations provided by Iran Water Resources Management Co. (IWRM) (Fig. 1*b*). The gauge observed rainfall datasets have been quality checked and screened by IWRM prior to making it available. They analyze the rainfall data by using a multivariate regression method between adjacent rain gauges. Then, statistical tests are conducted to check the data consistency. It is noted that the quality assurance of rain gauge data is beyond the scope of this research, and thus, is not addressed here. The interested readers are referred to the publications discussed by Draper and Smith (1998), You et al. (2007), and Mathes et al. (2008).

The required surface rainfall data are derived from forty rain gauges distributed across the twenty pixels of the study area to evaluate satellite precipitation products during the sixty rainy days in the period from 22 November 2003 to 22 May 2006. Note that all the sixty events occur in the winter and spring which are the rainy seasons over Khuzestan. Hence, the study period consists of eighteen months including six months of the winter and spring seasons at each year (2003–2006).

It should be noted that the satellite-retrieved precipitation is continuous and represents an areal rain rate at each pixel, while the gauge observed rainfall is at a particular point in a location. Therefore, to make comparisons between the two sources, pixels where gauges are available are selected across the study area. The areal reference rainfall over a pixel size is considered the rainfall value measured by the rain gauge located within that pixel. Also, for a pixel with two or more rain gauges, the areal reference rainfall is obtained based on the average value of those rain gauges located within that pixel.

The satellite rainfall products used in this study are based on Precipitation Estimation from Remote Sensing Information using Artificial Neural Network (PERSIANN) (Sorooshian et al., 2000) and Tropical Rainfall Measuring Mission (TRMM) Multi-satellite Precipitation Analysis (TMPA) adjusted product (3B42). The PERSIANN system uses neural network function classification/approximation procedures to compute an estimate of rainfall rate at each 0.25° × 0.25° pixel of the infrared brightness temperature image provided by geostationary satellites. An adaptive training feature facilitates updating of the network parameters whenever independent estimates of rainfall are available. The PERSIANN system was based on geostationary infrared imagery and later extended to include the use of both infrared and daytime visible imagery. Rainfall products are available from 50°*S* to 50°*N* globally.

TMPA provides global precipitation estimates from a wide variety of meteorological satellites (Huffman et al., 2010). Indeed, the TMPA estimates are available in the form of two products, a near real-time version (3B42RT) (about 6 h after real time) covering the global latitude belt from 60°*N* to 60°*S* and a gauge-adjusted post-real-time research version (3B42) (approximately 10–15 days after the end of each month) within the global latitude belt ranging between 50°*N* and 50°*S*. Both 3B42RT and 3B42 have 3-hour temporal and 0.25° × 0.25° spatial resolution. The 3B42RT uses the TRMM Combined Instrument (TCI) dataset, which includes the TRMM precipitation radar (PR) and TRMM Microwave Imager (TMI), to calibrate precipitation estimates derived from available Low Earth Orbit (LEO) microwave (MW) radiometers. The 3B42RT then merges all of the estimates at 3-hour intervals; and the gaps in the analyses are filled using Geostationary Earth Orbit (GEO) infrared (IR) data regionally calibrated to the merged MW

product. The 3B42 adjusts the monthly accumulations of the 3-hour fields from 3B42RT based on a monthly gauge analysis, including the Global Precipitation Climatology Project (GPCP) (Gebremichael et al., 2005) 1° × 1° monthly rain gauge analysis and the Climate Assessment and Monitoring System (CAMS) 5° × 5° monthly rain gauge analysis (Jiang

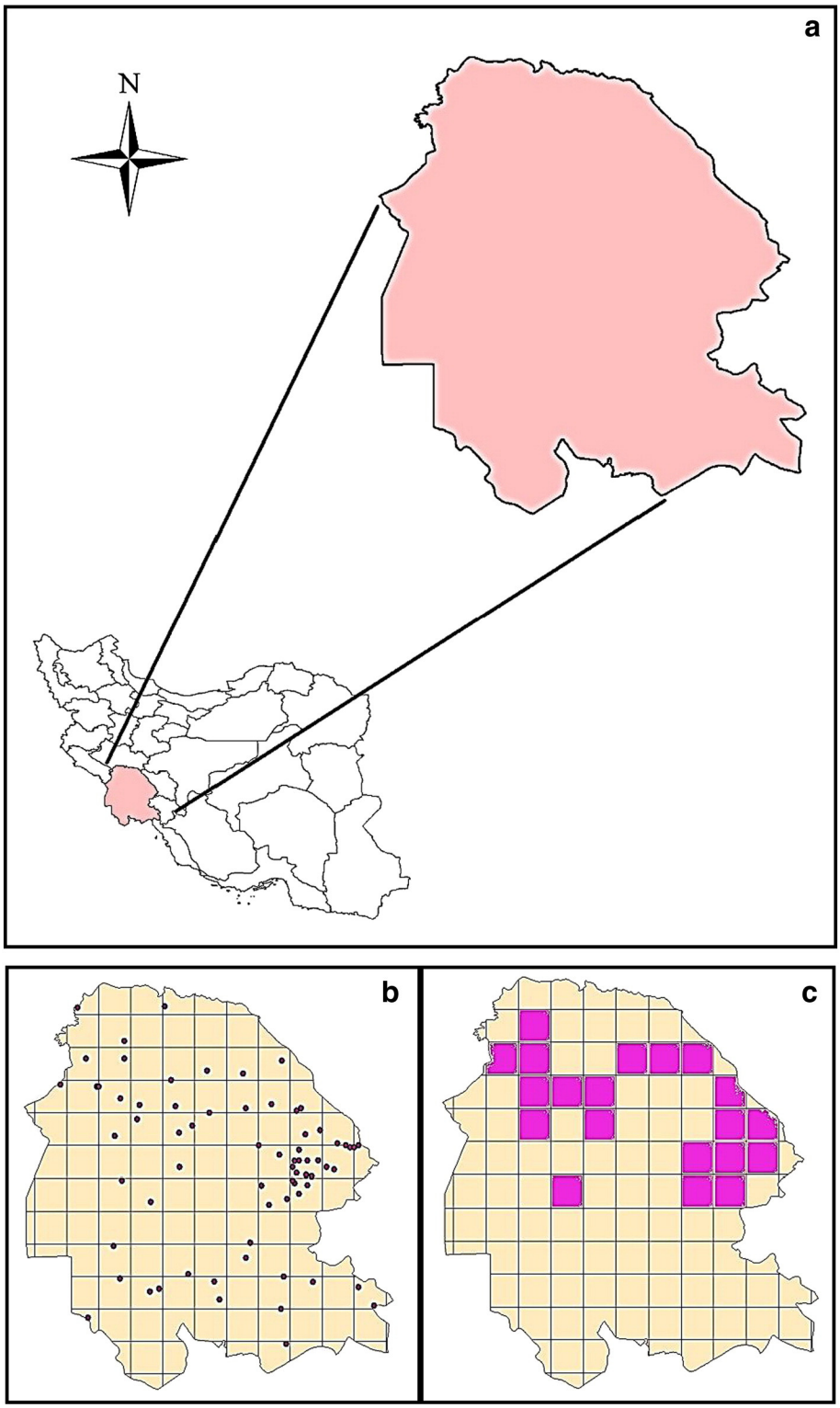

Fig. 1. Study area: (a) Khuzestan Province in the southwest of Iran, (b) rain gauges and satellite pixels over Khuzestan Province, (c) selected satellite pixels for study over Khuzestan Province.

et al., 2012). Note that the daily satellite rainfall data employed in the current work are computed by aggregating 3-hour temporal resolution data over 24-h for both PERSIANN and TMPA-3B42 products.

It is worth pointing out that the SREs at any given point are dependent on a number of factors, some of which are independent of geography. For example, TMPA-3B42RT employs multiple microwave sensor combinations with gaps filled with IR-based estimates, while PERSIANN is mainly based on one input data set (Infrared (IR) brightness temperature calibrated with microwave observations). Thus, PERSIANN is expected to have more homogeneous errors than TMPA-3B42RT (Aghakouchak et al., 2012).

3. Methodology

In the presented model, at first, the multiple uncertainty fields associated with satellite rainfall estimates are simulated using copula-based random generation of observed biases. Then, in order to obtain an ensemble of bias-adjusted rainfall realizations of satellite estimates, the simulated multiple uncertainty fields are imposed over the original satellite estimates. Fig. 2 provides a general overview of the proposed model; however, all the steps of simulation are presented briefly as follows:

1) A number of sixty daily rainfall events are selected, each of which is concurrent over the twenty 0.25° × 0.25° pixels. All the sixty events show a positive value of rain rate according to the rain gauge observations. It is noted that the fifty-four out of sixty (90%) events in all the twenty pixels are employed in order to simulate the ensembles of bias fields and a number of six events (10%) are left to examine the reliability of the simulated model.
2) The difference between rain gauge measurements as reference surface rainfall data and SRE at each pixel is considered and termed as observed bias. The value of observed bias is obtained for each event at each selected pixel separately. Now, we have a 54-by-20 matrix of observed bias values.
3) The best probability distribution function (PDF) is fitted to the observed bias values of each pixel; subsequently, the cumulative distribution functions (CDFs) of the biases are computed for each pixel (a 54-by-20 matrix of values in the open interval (0,1) for twenty pixels).
4) The n-dimensional multivariate Gaussian copula is fitted to the computed CDF from the previous step. Since the bias at each pixel is assumed as a variable, the dimensionality (n) of the Gaussian copula for the twenty pixels used in this study is twenty. Indeed, copula can model the dependencies by describing the joint multivariate distribution; hence, the spatial dependence structure of bias values among different pixels can be modeled by copula.
5) Gaussian copula is employed to generate an ensemble of CDFs randomly based on the observed CDFs.
6) Ensembles of bias fields that are equal to inverse values of randomly generated CDFs are obtained. Using copula, one can simulate random variables (here random biases from different pixels) with the same probability distribution as that of the input data (here observed biases from different pixels), while preserving the dependence structure of the variables (Nelsen, 2006).
7) The outlier data of the randomly generated ensembles of biases are detected and removed.
8) The simulated multiple random bias fields are imposed over the original satellite estimates of an event in order to obtain an ensemble of bias-adjusted realizations of SREs for that event.
9) An uncertainty analysis technique (see Section 3.5) is employed in order to measure the strength of the simulated ensembles with respect to uncertainty prediction.
10) As mentioned before, a number of six daily events which have not participated in the ensembles simulation of bias fields are employed to examine the reliability and performance of the developed model. Furthermore, the simulated realizations are evaluated using three statistical indices including bias, root mean square error (RMSE), and correlation coefficient (CC).

Further explanations of the above-mentioned steps are discussed in the following sections.

3.1. Evaluation of SREs bias

The bias of SREs is calculated by comparing the rainfall estimates derived from the satellite algorithms (PERSIANN and TMPA-3B42) with the rain gauge observations as reference data. The evaluation is conducted over a domain including the twenty 0.25° × 0.25° pixels. The required statistical indices to evaluate SREs are computed at each selected pixel by Eqs. (1) to (4).

$$Bias = \frac{\sum_{i=1}^{N}\left(P_{O_i} - P_{S_i}\right)}{N} \tag{1}$$

$$RMSE = \left[\frac{\sum_{i=1}^{N}\left(P_{S_i} - P_{O_i}\right)^2}{N}\right]^{1/2} \tag{2}$$

$$CC = \frac{\sum_{i=1}^{N}\left(P_{S_i} - \overline{P}_S\right)\left(P_{O_i} - \overline{P}_O\right)}{\sqrt{\sum_{i=1}^{N}\left(P_{S_i} - \overline{P}_S\right)^2}\sqrt{\sum_{i=1}^{N}\left(P_{O_i} - \overline{P}_O\right)^2}} \tag{3}$$

$$RBias = \frac{\sum_{i=1}^{N}\left(P_{O_i} - P_{S_i}\right)}{\sum_{i=1}^{N} P_{O_i}} \times 100\% \tag{4}$$

Where P_{S_i} and P_{O_i}, respectively, are the values of SRE and rain gauge observation for the ith event, N is the number of daily events, $\overline{P}_S$ and $\overline{P}_O$, respectively, are the average value of

SREs and rain gauge observations for N daily events over each pixel.

3.2. General concept of copula

Copulas are joint cumulative distribution functions that describe dependencies among variables independent of their marginal (Joe, 1997; Nelsen, 2006). Consider p uniform $u(0,1)$ random dependence variables $U_1, \ldots, U_p$. The relationship between these random variables is defined through their joint distribution function as follows:

$$C\left(u_1, \ldots, u_p\right) = Pr\left(U_1 \le u_1, \ldots, U_p \le u_p\right). \quad (5)$$

Function C is called a copula. To complete the definition, let $(X_1, \ldots, X_p)$ indicate a set of n random variables and $(x_i, \ldots, x_p)$ a realization of it. Then copula is a function that links the multivariate distribution $F(x_1, \ldots, x_p)$ to its univariate marginals $F_{X_i}(x_i)$. Sklar (1959) demonstrated that:

$$C\left(F_{X_1}(x_1), \ldots, F_{X_p}\left(x_p\right)\right) = F\left(x_1, \ldots, x_p\right) \quad (6)$$

$$C : [0,1]^n \rightarrow [0,1]. \quad (7)$$

In the copula model defined in Eq. (6), it is possible to integrate different families of probability distributions for each outcome. This is the main advantage of this approach compared to standard multivariate models used in practice (Favre et al., 2004). In addition, copula can preserve the dependencies among variables that are described with a correlation n-by-n matrix where n is the number of variables. Fig. 3 illustrates the concept of copula schematically.

3.2.1. Gaussian copula

Gaussian copula as a member of the Elliptical copula is the most commonly used copula family, especially to model dependence structures. The key advantage of Gaussian copula is that one can specify different levels of correlation between the marginals. In addition, it is practically manageable and simple (Fang, 2012). This copula uses a symmetric and positive definite matrix in order to model dependence. The elements of this matrix can be interpreted as dependence measures between couples of variables, leading to an analogy with the correlations used in the case of multivariate Gaussian distributions. This model is thus convenient when the number of dimensions is more than two or three (Renard and Lang, 2007). Several studies also have highlighted the application of Gaussian copula to describe the dependence between variables in multivariate distributions (Song, 2000; Renard and Lang, 2007; Madsen, 2009; Song et al., 2009; Aghakouchak et al., 2010a,b,c; Fang, 2012). However, since the Gaussian copula does not have upper or lower tail dependence, it may not be a suitable choice for modeling the dependencies of extremes (Schmidt, 2005; Frahm et al, 2005; Schmidt and Stadtmuller, 2006; Serinaldi, 2009a,b; Aghakouchak, 2010). If tail dependence is observed in the data, alternative copula families, for instance the t-copula may be more appropriate. In principle, the choice of the more suitable copula for modeling a data set is not straightforward, especially if the data set is not informative enough to provide relevant indications about the asymptotic dependence properties (Renard and Lang, 2007). Consequently, in this study, as a first attempt to quantify and adjust the uncertainty associated with SREs over a developing region in Iran with inadequately informative data set of observations, a multivariate Gaussian copula that is relatively easy to handle is

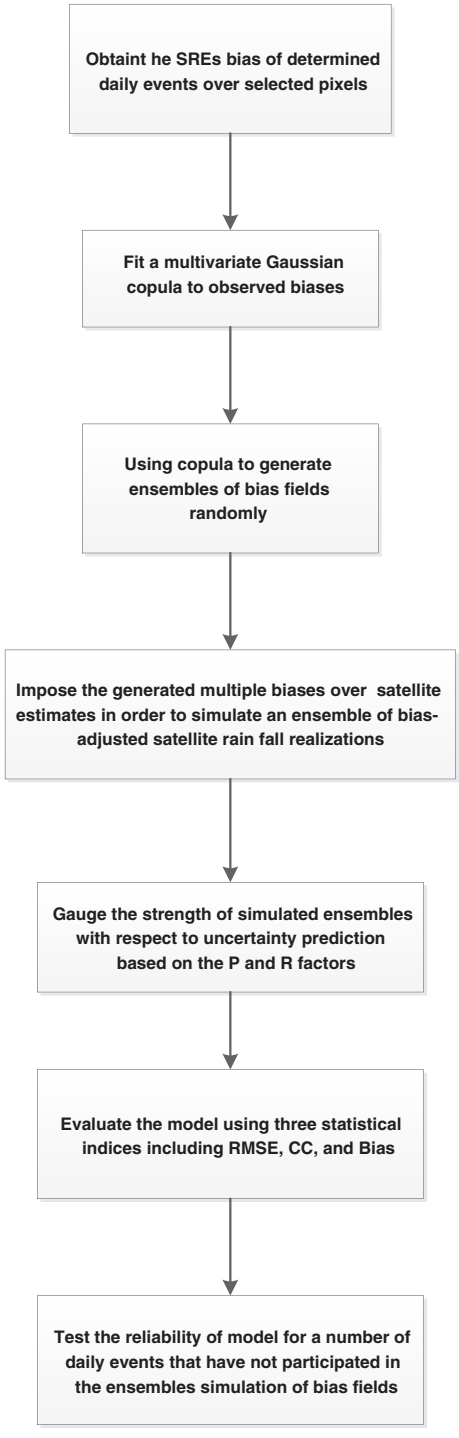

Fig. 2. Flowchart of research procedure.

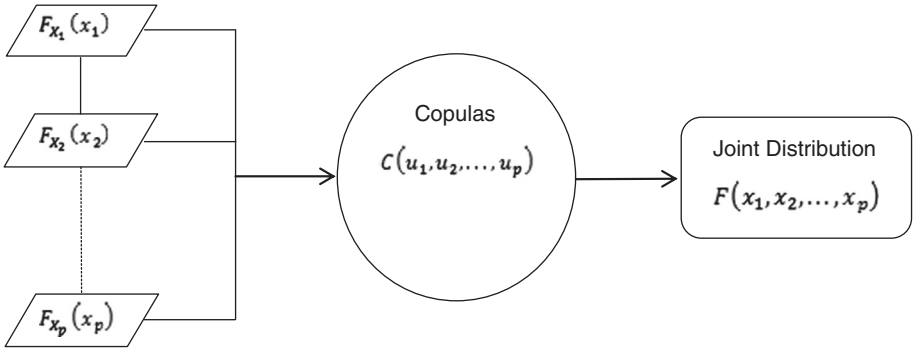

Fig. 3. A schematic diagram of copula (Favre et al., 2004).

employed to describe the dependence structures and to simulate multivariate satellite rainfall bias fields. The *n*-dimensional multivariate Gaussian copula is derived from the multivariate normal distribution (Nelsen, 2006) and described with a correlation matrix $\rho_{n\times n}$ (n is the number of variables) as follows:

$$C_\rho^n(u_1,\ldots,u_n) = F_\rho^n\left[F^{-1}(u_1),\ldots,F^{-1}(u_n)\right] \tag{8}$$

Where u_i is the ith random vector and F_ρ^n is multivariate standard Gaussian distribution function whose density function is:

$$c(u_1,\ldots,u_n) = \frac{1}{\sqrt{det(\rho)}}exp\left[-\frac{1}{2}y(u)^{'}\left(\rho^{-1}-I\right)y(u)\right] \tag{9}$$

Where $y(u_i) = F^{-1}(u_i)$, *det* is determinant, and *!* is transpose operation.

3.3. Copula-based simulation

Let C^n be the copula of a multivariate *n*-dimensional distribution $H \equiv (H_1, \ldots, H_n)$ where $H_1, \ldots, H_n$ are the marginal distributions. In order to obtain a simulated field of $x \equiv (x_1, \ldots, x_n)$ with marginals of $H_1, \ldots, H_n$, the following three steps are required:

1) Estimate the parameter of the copula C^n.
2) Simulate uniform random variables $u(u_1, \ldots, u_n)$ using the copula C^n.
3) Transform the univariate marginals to $H_1, \ldots, H_n$ using Sklar's theorem (Sklar, 1959): $x_i = H_i^{-1}(u_i)$.

It is noted that $H_1, \ldots, H_n$ do not necessarily need to have the same distribution family (Aghakouchak, 2010). As mentioned previously, since copula is invariant to monotonic transformations of the variables, the simulated random variables will have the same spatial dependence structure as that of input data. This is one of the main advantages of copula in the simulation of spatially dependent random fields. In the present study, the copula parameter is estimated based on the observed biases at each pixel.

3.4. Simulation of an ensemble of bias-adjusted rainfall realizations

In this research, as mentioned before, the observed biases of fifty-four daily rainfall events over twenty pixels are employed as input data to copula-based model. The bias at each pixel is considered as a variable, and thus a multivariate twenty-dimensional Gaussian copula for twenty pixels is implemented in order to generate multiple random bias fields. The marginal distribution of each variable is constructed based on a parametric approximation which uses Anderson–Darling goodness-of-fit test in order to fit the best probability distribution function (PDF) to each variable. This criterion has demonstrated good skills in hydrological applications (Laio, 2004; Laio et al., 2009; Di Baldassarre et al., 2009). Also, the parameters of each distribution are obtained by using Maximum Likelihood Estimation (MLE) method. The specific PDF associated with the observed biases at each pixel and the related values of parameters are provided in Appendix A.

The correlation parameter of multivariate Gaussian copula is estimated based on the observed biases as follows:

(1) Estimate the marginal cumulative distribution functions as described before.
(2) Generate Gaussian values by applying the inverse of the normal distribution to the empirical distribution functions.
(3) Compute the linear correlation matrix of the transformed data (Cherubini et al., 2004).

Using multivariate Gaussian copula, a set of one thousand members of bias fields is generated randomly for each pixel. Then, the outlier data are removed from the generated biases. The outlier data are detected based on the statistical methods for multivariate outlier detection. These methods often indicate the outliers as those data that are located relatively far from the center of the data distribution. Several distance measures can be implemented for such a task. In this study the Mahalanobis distance as a well-known criterion for the detection of multivariate outliers is used. The Mahalanobis distance depends on estimated parameters of the multivariate distribution (Ben-Gal, 2005). Since the focus of this study is on the performance of the copula-based bias adjustment model, the details of outlier detection procedure are not included here. The interested readers are referred to the original publications discussed by Werner (2003), Hodge

and Austin (2004), Ben-Gal (2005), and Filzmoser (2005). After the outliers were detected and removed, the generated biases are imposed on the original satellite rainfall estimate (hereafter OSRE that refers to rainfall estimate by satellite products (PERSIANN and TMPA-3B42) before any adjustment of bias through the developed model in the current study) in order to obtain an ensemble of bias-adjusted rainfall realizations of satellite estimate (hereafter BASRE that refers to bias-adjusted satellite rainfall estimation products using developed model in this study) at each pixel.

Eq. (10) describes the general formulation of the presented method:

$$P_{BASRE_i} = P_{OSRE_i} + Bias_i \tag{10}$$

Where P_{BASRE_i} is an ensemble of bias-adjusted satellite rainfall realizations at ith pixel, P_{OSRE_i} is the OSRE at ith pixel, and $Bias_i$ is the randomly generated bias fields based on the fifty-four observed biases ($P_{O_i} - P_{S_i}$, see Eq. (1)) at ith pixel. It is pointing out that two types of error models including the additive error (*Bias*) model and the multiplicative error (*Mbias*) model are commonly used for the study of precipitation measurements. Many studies of satellite-based precipitation data products have used the additive error model ($Bias = \frac{1}{N}\sum_{i=1}^{N}(P_{O_i} - P_{S_i})$ (Shrestha, 2011)) (Ebert et al., 2007; Habib et al., 2009; Roca et al., 2010; Aghakouchak et al., 2012), while other studies such as Hossain and Anagnostou (2006), Ciach et al. (2007), and Villarini et al. (2009) have used the multiplicative model ($Mbias = \frac{\frac{1}{N}\sum_{i=1}^{N} P_{S_i}}{\frac{1}{N}\sum_{i=1}^{N} P_{O_i}}$ (Shrestha, 2011)) to quantify or simulate errors in radar- or satellite-based measurements. In fact, the use of different error models leads to different definitions and calculations of uncertainties (Tian et al., 2013). In the current study the additive bias model is employed to simulate biases of satellite-based rainfall estimates (the rainfall uncertainty is assumed to be an additive term). Note that in the framework proposed here, for a single "hit" (both rain gauge and satellite report positive rainfall values) event, one can correct the bias value by using both the additive and multiplicative models. However, for a single "miss" (rain gauge reports positive rainfall value, while satellite reports zero value) event, using the multiplicative model results in an indeterminate form (0/0) of bias-adjusted field. Therefore, in the case of "miss" event, the additive model may lead to more accurate estimation of bias-adjusted rainfall value. It should be noted that in this study, all the selected daily events have positive values of observed rainfall; however, the satellite data can be either positive or zero. Also, if the rainfall value becomes negative after bias adjustment, it will be set to zero.

3.5. Calibration and uncertainty analysis procedure

In this study an ensemble approach is used to describe the uncertainty associated with BASRE. The output uncertainty is quantified by the 80 percentage prediction uncertainty band (80PPU) calculated at the 10% lower and 90% upper limit levels of the simulated ensemble. The 80PPU band is used here, because we expect that the observed data fall within this band and not consider 20% of the inappropriate simulations. It is noted that in the several literatures (Abbaspour et al., 2004, 2007; Schuol et al., 2008; Yang et al., 2008) the 95PPU band calculated at the 2.5% lower and 97.5% upper limit levels of the output variables was used; however, in our case after a trade-off between different percentages, the 80PPU was selected as an appropriate band.

In stochastic simulations that predicted output is given by a prediction uncertainty band two different indices including *P*-factor and *R*-factor can be used to compare observations with simulations (Abbaspour et al., 2007). In the present research, *P*-factor and *R*-factor are computed in order to gauge the strength of the simulated ensembles with respect to uncertainty prediction. Here, the *P*-factor is the percentage of pixels bracketed by the 80PPU band. For example, the *P*-factor of 50% indicates that the 80PPU band of simulated ensemble brackets the observed values of ten pixels (here, the total number of studied pixels is twenty). The maximum value for the *P*-factor is 100% that ideally brackets all the observed data in the 80PPU band. The *R*-factor is calculated as the ratio between the average thickness of the 80PPU band and the standard deviation of the observed data. It expresses the width of the uncertainty interval and the smaller *R*-factor implies that the simulations are closer to the observations. Indeed, *R*-factor indicates the strength of the simulation and ideally can be smaller than 1; however, in the practical studies the reasonable value for *R*-factor is 1 that demonstrates the simulated fields match best with the standard deviation of observed data. The R-factor is calculated as:

$$R\text{-}factor = \frac{\frac{1}{n}\sum_{i=1}^{n}\left(Y_{i,90\%} - Y_{i,10\%}\right)}{\sigma_{obs}}$$

Where $Y_{i,90\%}$ and $Y_{i,10\%}$ represent the upper and lower boundary of the 80PPU at each pixel, n is the number of pixels (here 20), and σ_{obs} stands for the standard deviation of the observed rainfall value of a single daily event for all the twenty pixels (Abbaspour et al., 2007).

The goodness of calibration and prediction uncertainty is judged based on the closeness of the average value of *P*-factor to 100% and *R*-factor to 1 (Schuol et al., 2008; Yang et al., 2008). As a larger *P*-factor leads to a larger *R*-factor, often a trade-off between the two must be sought.

It is noted that, both *P* and *R* factors are calculated for a simulated ensemble of BASRE associated with a single daily event. However, there are fifty-four daily events here as input data to copula-based model; thus, after computing the values of *P*-factor and *R*-factor for each simulated ensemble of a daily event, one can obtain the average value of each factor for fifty-four daily events. In the model presented here, the above-mentioned steps are implemented for several sets of randomly generated bias fields; consequently, for each set of generated biases the average values of *P*-factor and *R*-factor for fifty-four simulated ensembles are computed. Therefore, the several pairs of averaged *P* and *R* factors are obtained. Then, an appropriate set among the different sets of randomly generated biases is selected based on the best values of both *P* and *R* factors. In fact, the selected set can simulate an ensemble of BASRE that has two features simultaneously: (Abbaspour et al., 2007) The 80PPU band brackets most of the observed data

(closer *P*-factor to 100%), and (AghaKouchak et al., 2009) the average distance between the upper (at 90% level) and lower (at 10% level) parts of the 80PPU is as small as permissible that indicates a better correspondence between simulation and observation fields (closer *R*-factor to 1).

4. Results and discussion

The main objective of this study is to develop a model for adjusting biases of two widely-used SRE products over an important region in Iran. However, before displaying any analysis results of the proposed model, a brief evaluation of both satellite precipitation products across the study area is presented. The evaluation is implemented during a period of three years (2003–2006) including six rainy months (winter and spring seasons) in each year over twenty 0.25° × 0.25° pixels. Fig. 4, compares the time series of daily precipitation for both SREs and rain gauge observations during the six rainy months in each year of the three years studied period separately. In this figure, the rainfall value for each day is the average value of twenty pixels in that day (vertical axis). As seen in Fig. 4, TMPA-3B42 demonstrates better estimates than PERSIANN. In addition, three continuous statistical indices including *RMSE*, *CC*, and *RBias* (Eqs. (2) to (4)) are computed in order to evaluate both satellite rainfall products over the study area. Also, in order to assess the rain detecting skill of SREs, two categorical statistical indices (Wilks, 2006) including the probability of detection (*POD*) and false alarm ratio (*FAR*) are used (Eqs. (12) and (13)). The *POD* represents the ratio of the correct identifications number of rainfall by satellite product to the total number of rainfall occurrences observed by reference data. FAR denotes the fraction of cases in which the satellite records rainfall when the rain gauges do not. *POD* and *FAR* range from 0 to 1, with 1 being a perfect *POD* while 0 being a perfect *FAR*. In this section, both continuous and categorical statistical indices are obtained based on the daily precipitations during the eighteen months.

$$POD = \frac{t_H}{t_H + t_M} \tag{12}$$

$$FAR = \frac{t_F}{t_H + t_F} \tag{13}$$

Where *H*, *M*, and *F* are different cases: *H*, observed rain correctly detected; *M*, observed rain not detected; *F*, rain detected but not observed; and t_H, t_M, and t_F are the times of occurrence of the corresponding case (Jiang et al., 2012). It is noted that in this study, a threshold of 1.0 mm/day is used to distinguish between rain and no rain. Fig. 5 displays the scatterplots of daily SREs versus gauge observations during eighteen months. The statistical indices shown in this figure are the daily averaged value during eighteen months over the twenty selected pixels. As seen in Fig. 5, the values of CC and RBias for TMPA-3B42 are better than PERSIANN, but in terms of *RMSE*, *POD*, and *FAR*, both products represent similar results. In general, based on the obtained results in this section, TMPA-3B42 indicates more accurate estimates than PERSIANN. Note that the results presented in both Figs. 4 and 5 are based on the comparison between original SREs (before any adjustment of bias through the developed model in the current study) and rain gauge data. Since the focus of this study is on the assessment of the copula-based bias adjustment model, the related results are presented in the following sections.

4.1. Evaluation of bias-adjusted SREs

In order to assess the accuracy of the simulated ensembles, three types of continuous statistical indices including *Bias*, *RMSE*, and *CC* are used. These indices are computed for both original (OSRE) and bias-adjusted (BASRE) estimates of satellite precipitation products separately by comparing them with the rain gauge observations as reference data. Figs. 6 and 7 provide the values of three indices for both PERSIANN and TMPA-3B42 products, respectively. Note that all the three indices in this section are computed for the fifty-four daily events over the twenty pixels. As discussed before, an ensemble of BASRE of a daily event is simulated by imposing copula-based randomly generated bias fields over the OSRE of that event. Thus, for fifty-four selected daily events, a set of fifty-four ensembles will be simulated, each of which consists of a large number of realizations. Each of realizations represents a possible daily rainfall event that can occur over the studied domain. Consequently, in Figs. 6 and 7, the values of three indices (*Bias*, *RMSE*, and *CC*) associated with the original estimates (OSRE) are the average values of fifty-four daily events over each pixel, also, the values associated with the bias-adjusted estimates (BASRE) are the average values of 50% quantiles of fifty-four bias-adjusted ensembles (each ensemble with around one thousand members has a value of 50% quantile) over each pixel. As seen in Figs. 6 and 7, for all three indices the estimates of both PERSIANN and TMPA-3B42 are improved after bias adjustment. Table 1 contains the average values of statistical indices over twenty pixels and shows the improvement percentage of each index for both PERSIANN and TMPA-3B42 products.

It should be noted that throughout this paper, in order to simulate an ensemble of BASRE, the outliers are removed from the randomly generated biases before they are imposed over OSRE (see Section 3.4).

4.2. Copula-based bias simulation

As previously mentioned, in this study, a twenty-dimensional multivariate Gaussian copula is employed to generate bias fields of SREs randomly over twenty pixels. Since copulas are invariant to monotonic transformations, the simulated random biases will have the same spatial dependence structure as that of the observed biases. To show the spatial dependency preserved by copula, a comparison between the scatterplots of the observed and copula-based randomly generated biases for two pixels with the highest and lowest correlation coefficient is displayed in Figs. 8 and 9. Moreover, the CC values of bias between each pair of pixels for all the twenty pixels are provided in Tables B1 and B2 of Appendix B. With respect to the PERSIANN product, the highest *CC* values between two pixels (pixels number 6 and 12 in Table B1) for the observed and generated biases are 0.96 and 0.97, respectively, while these values for TMPA-3B42 product are 0.89 and 0.91 (pixels number 10 and 11 in Table B2). However,

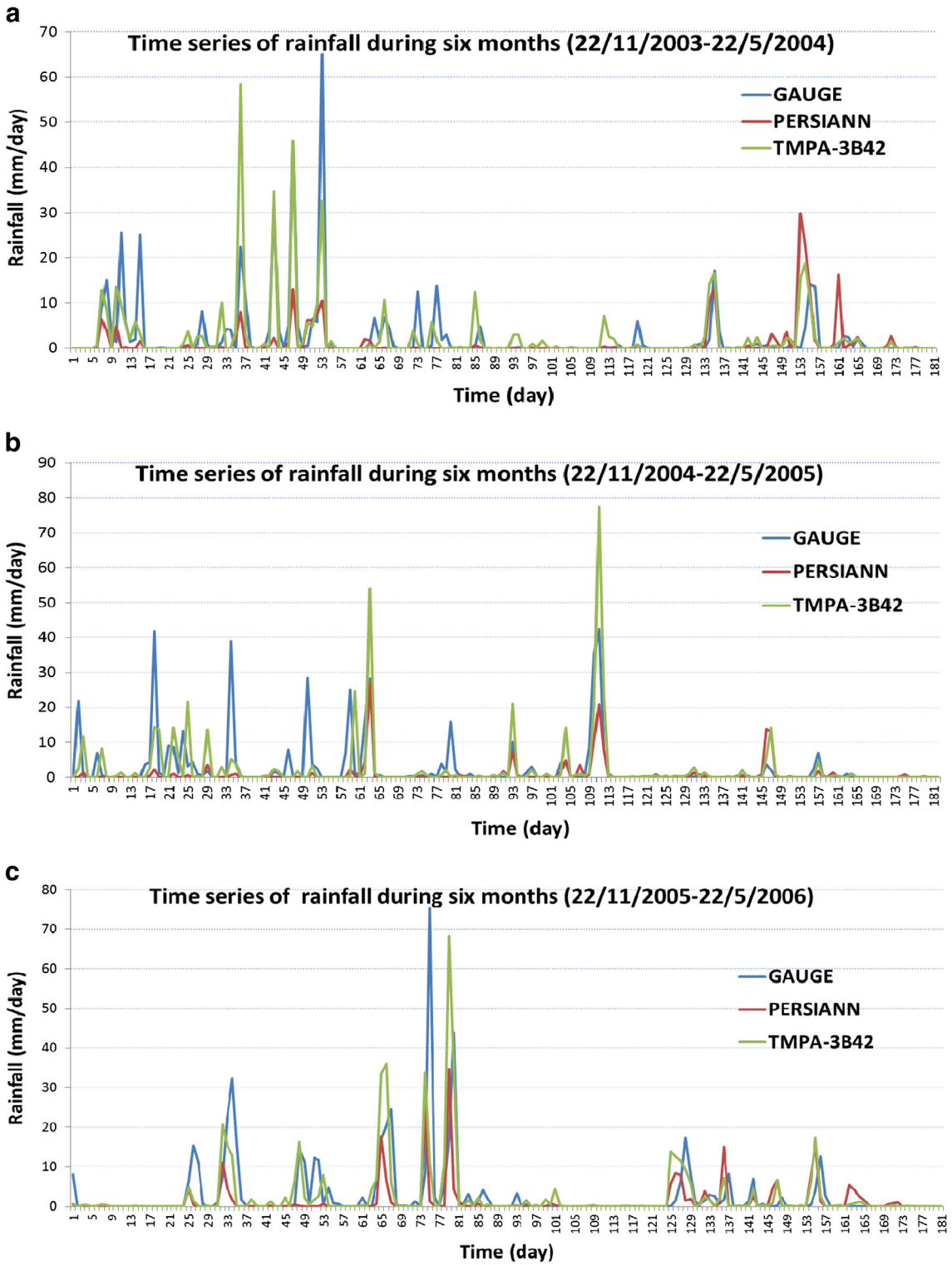

Fig. 4. Average daily variations of rainfall over twenty pixels, derived from rain gauges and estimates by PERSIANN and TMPA-3B42 products during six rainy months of: (a) the first year, (b) of the second year, and (c) of the third year of study period.

for PERSIANN the lowest CCs between two pixels for the observed and generated biases are 0.43 and 0.49 (pixels number 2 and 19 in Table B1), respectively, and for TMPA-3B42 they are 0.09 and 0.16 (pixels number 8 and 20 in Table B2). As shown in these figures, the correlations between the observed biases (marked with red symbols) are reasonably preserved in the

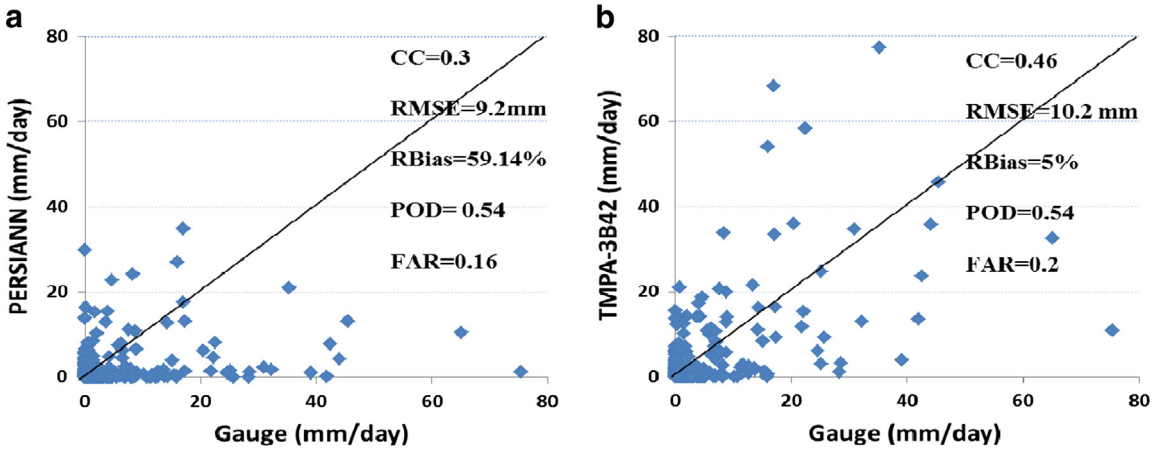

Fig. 5. Scatterplots of daily SREs versus gauge observations, spatially averaged over twenty pixels during eighteen rainy months of the three years study period: (a) PERSIANN estimates versus rain gauges observations (b) TMPA-3B42 estimates versus rain gauge observations.

generated biases (marked with blue symbols) for both highest and lowest values of *CC* between two pixels. Furthermore, the scatterplots of the bias values between previously mentioned pixels for the six validation events are presented in Figs. 8 and 9 (marked with green symbols). Note that the values of *CC* associated with the six validation events for PERSIANN in Fig. 8*a* and *b* are 0.97 and 0.78, respectively, while for TMPA-3B42 in Fig. 9*a* and *b*, they are 0.76 and 0.31. Considering the obtained results in this section, one can conclude that the copula simulation is done properly as the correlation is similar to that of the observations.

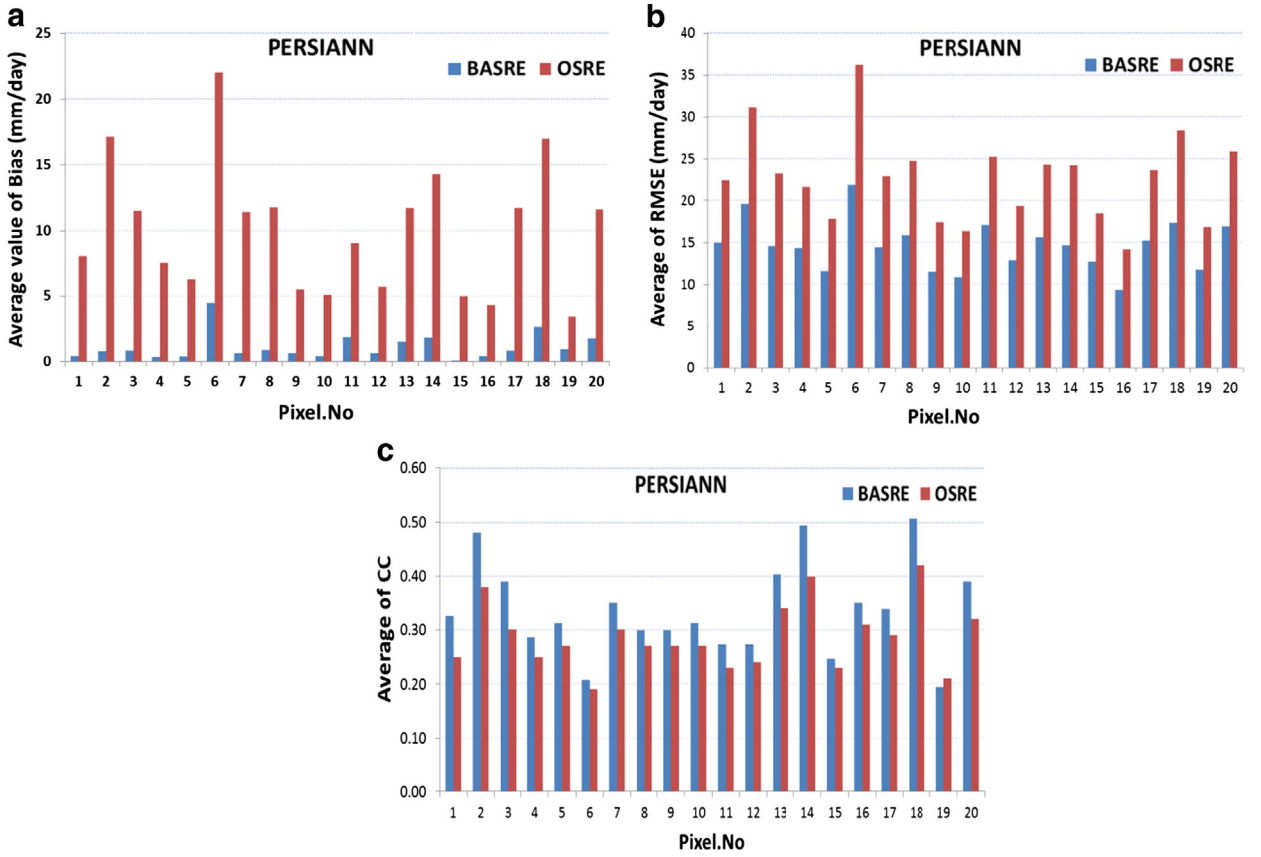

Fig. 6. Comparison between OSRE and BASRE (the 50% quantile of simulated realizations) of average values of (a) Bias, (b) RMSE, and (c) CC for fifty-four daily rainfall events over each pixel for PERSIANN product.

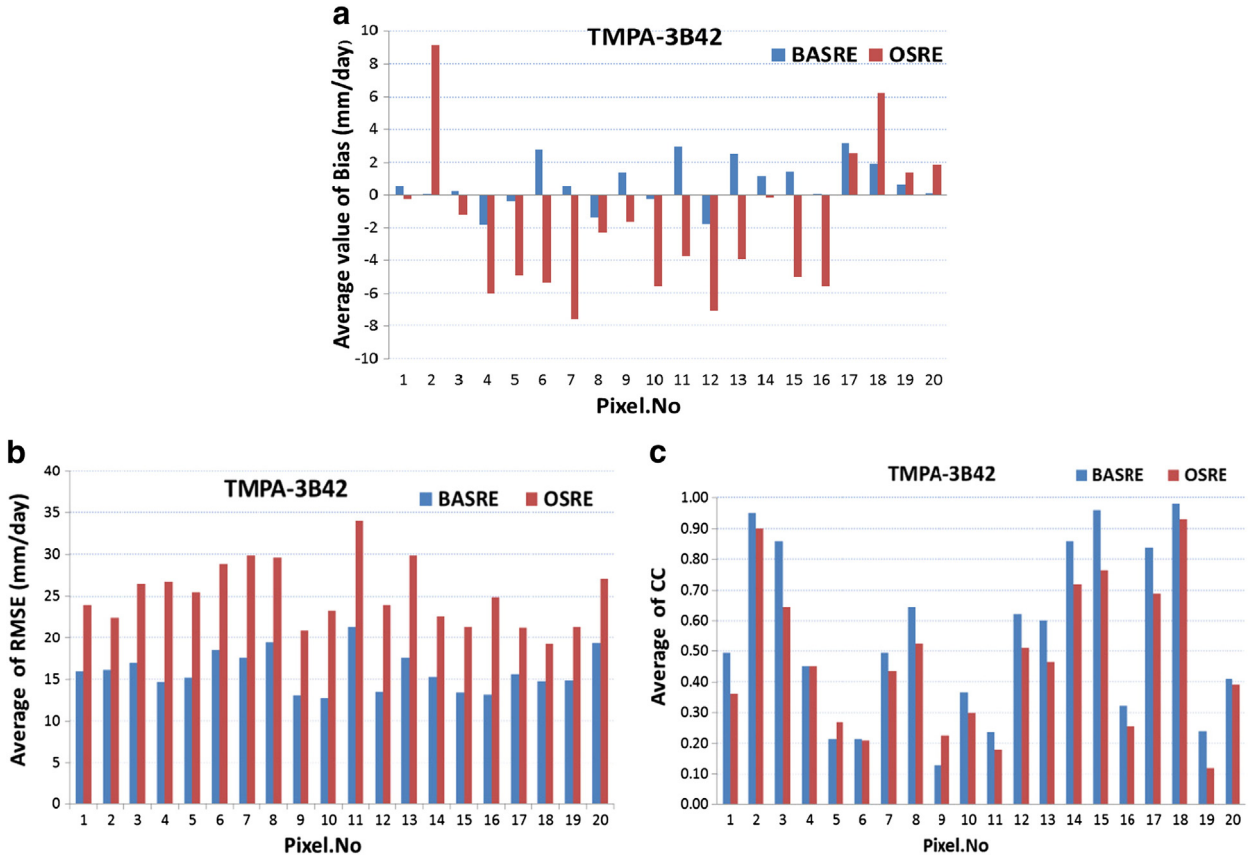

Fig. 7. Comparison between OSRE and BASRE (the 50% quantile of simulated realizations) of average values of (a) Bias, (b) RMSE, and (c) CC for fifty-four daily rainfall events over each pixel for TMPA-3B42 product.

4.3. Testing the developed model and uncertainty analysis

The reliability of copula-based bias adjustment model proposed in this study is tested for the six daily rainfall events which have not participated in the ensembles simulation. For this purpose, an appropriate set of generated biases (see Sections 3.4 and 3.5) is imposed on the OSRE associated with the six events in order to simulate six ensembles of BASRE of those events. It is noted that the average values of P and R factors for the selected set of generated biases are 65% and 1.85 for PERSIANN product, and 70% and 1.65 for TMPA-3B42 product. Then, for each event, the simulated ensemble is compared with the rain gauge observations. Tables 2 and 3 represent the average values of *RMSE* and *CC* of the six evaluated events over each pixel for PERSIANN and TMPA-3B42 products, respectively. Also, the bias value associated with each tested event at each pixel for both satellite products is exhibited in Tables 4 and 5. These indices are obtained for OSRE and BASRE by comparing them with rain gauge data separately. Notice that the indices for BASRE are computed based on the 50% quantile values of the simulated ensembles. As seen, all three indices are improved after bias adjustment of the satellite estimates. With respect to the values of P and R factors (Table 6) which are considered as a criteria to examine the strength of the simulated ensembles, one can see that the simulated realizations of BASREs of Event 3 (Plot (*c*)) among the six tested events demonstrate better agreement with the

Table 1
Comparison of the average values of statistical indices of fifty-four daily rainfall events over twenty pixels for the OSRE and BASRE (the 50% quantile of simulated realizations).

Satellite products	*Bias* (OSRE)	*Bias* (BASRE)	Improved *Bias* (%)	*RMSE* (OSRE)	*RMSE* (BASRE)	Improved *RMSE* (%)	*CC*(OSRE)	*CC*(BASRE)	Improved *CC* (%)
PERSIANN	10.01	1.16	88.41	22.73	14.68	35.42	0.29	0.34	17.24
TMPA-3B42	−1.95	0.70	64.10	25.18	15.95	36.66	0.47	0.54	14.89

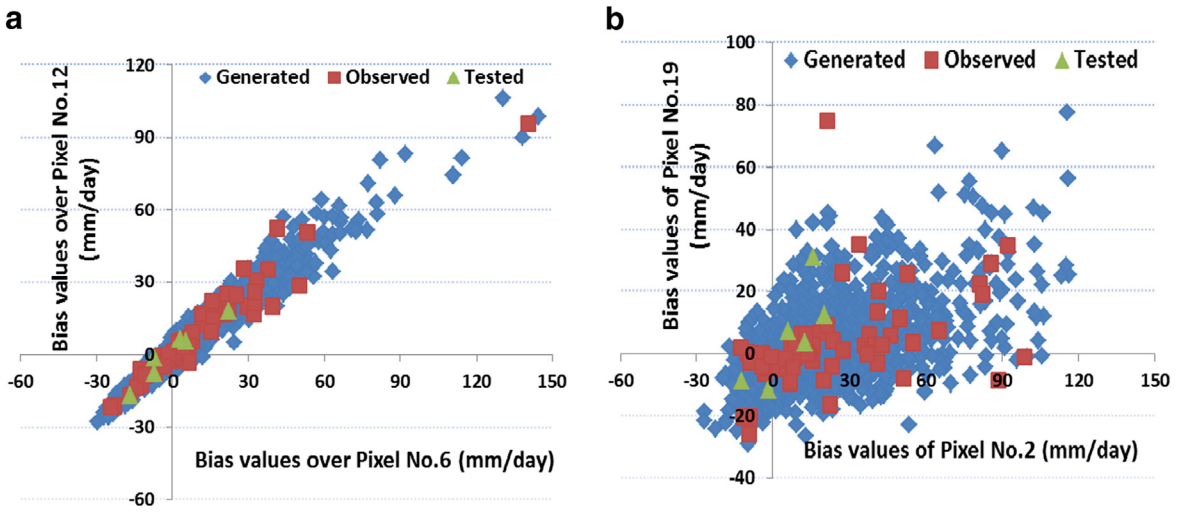

Fig. 8. Scatterplot of bias pairs for: the fifty-four observed events (red symbols), the six validation events (green symbols), and the generated samples by Gaussian copula (blue symbols) associated with PERSIANN product over (a) two pixels with the highest value of the correlation coefficient, and (b) two pixels with the lowest value of the correlation coefficient based on the observed events. (For interpretation of the references to color in this figure legend, the reader is referred to the web version of this article.)

observations for both PERSIANN and TMPA-3B42 products. Table 6 shows the computed *P* and *R* factors of six tested events for PERSIANN and TMPA separately. As displayed in this table, Event 3 with *P*-factor of 80% indicates that the 80PPU band of simulated ensemble brackets the observed values of sixteen pixels; also, the *R*-factor closer to 1 implies that simulations are more consistent with the observations. In addition, Figs. 10*a* to *f* and 11*a* to *f* for PERSIANN and TMPA-3B42 products, respectively, display the results of the simulated rainfall ensembles using Gaussian copula model for the six selected events over twenty pixels (each plot is associated with each event). In these figures, the solid red lines show the OSREs, the solid blue lines express the rainfall values derived from rain gauges, the gray areas represent the 80PPU bands (see Section 3.5) of the simulated realizations of BASREs, and the solid green lines indicate the 50% quintiles of simulated realizations. As shown, the BASREs using Gaussian copula (gray bands) reasonably encompass the ground reference measurements (solid blue lines). However, for each tested event there are a number of pixels where the observed data fall outside the simulated ensembles. The main reasons can be mentioned as follows:

(1) The number of input data (fifty-four daily events) used here may not be sufficient for simulations.

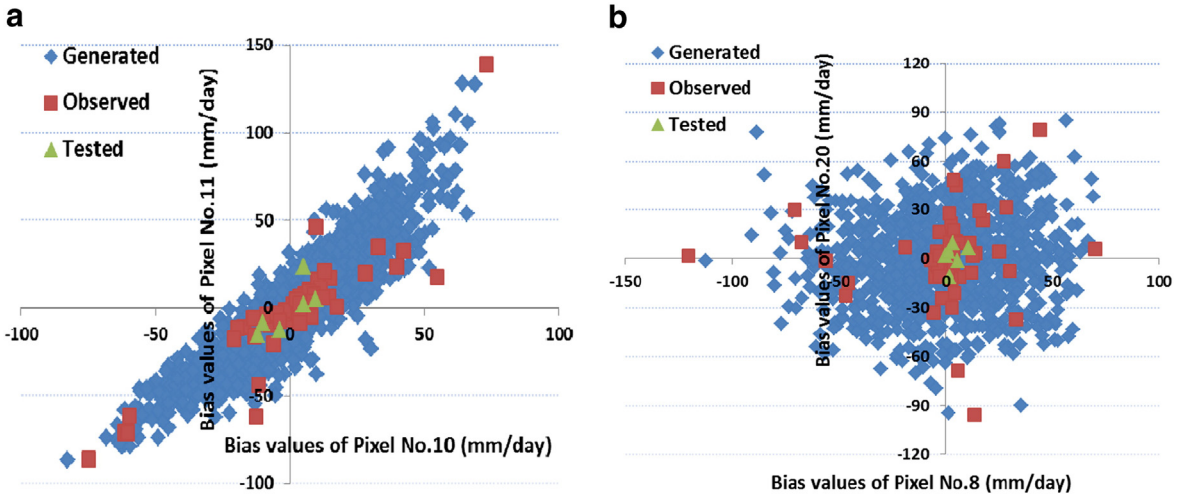

Fig. 9. Scatterplot of bias pairs for: the fifty-four observed events (red symbols), the six validation events (green symbols), and the generated samples by Gaussian copula (blue symbols) associated with TMPA-3B42 product over (a) two pixels with the highest value of the correlation coefficient, and (b) two pixels with the lowest value of the correlation coefficient based on the observed events. (For interpretation of the references to color in this figure legend, the reader is referred to the web version of this article.)

Table 2
Results of the average values of statistical indices of the six tested events over each pixel, comparison between the OSRE and BASRE (the 50% quantile of simulated realizations) for PERSIANN product.

Results of tested events (PERSIANN)				
Pixel. no	*RMSE*(BASRE)	*RMSE*(OSRE)	*CC*(BASRE)	*CC*(OSRE)
1	7.59	14.10	0.82	0.24
2	8.93	11.87	0.19	0.34
3	2.57	7.68	0.87	0.28
4	1.93	6.48	0.86	0.33
5	1.79	9.04	0.93	0.16
6	5.34	8.32	0.93	0.47
7	6.09	10.71	0.69	0.41
8	3.83	5.07	0.42	0.72
9	3.50	6.59	−0.13	0.56
10	1.75	7.24	0.83	0.29
11	4.43	6.31	0.70	0.44
12	5.64	9.80	0.32	−0.06
13	7.01	9.72	0.37	0.17
14	6.69	6.65	−0.16	−0.10
15	1.30	8.52	0.95	0.13
16	2.93	6.68	0.84	0.54
17	8.15	3.62	0.56	0.92
18	10.30	8.97	0.66	0.79
19	7.64	6.56	0.43	0.71
20	5.63	4.78	0.10	0.69
Average	5.15	7.94	0.56	0.40

(2) Input data are associated with two different seasons (winter and spring) which may lead to different types of storms.
(3) The quality assurance procedure employed on rain gauge data may also have played a role.

Therefore, to improve the simulation, one can implement the developed model by using a more reliable dataset of similar types of the rainfall observations at a fine temporal resolution (e.g. sub-daily) as input data.

Table 3
Results of the average values of statistical indices of the six tested events over each pixel, comparison between the OSRE and BASRE (the 50% quantile of simulated realizations) for TMPA-3B42 product.

Results of tested events (TMPA-3B42)				
Pixel. no	*RMSE*(BASRE)	*RMSE*(OSRE)	*CC*(BASRE)	*CC*(OSRE)
1	6.10	9.45	0.85	0.38
2	4.68	12.17	0.95	0.84
3	3.07	3.84	0.79	0.34
4	2.19	6.21	0.93	0.48
5	1.44	5.81	0.97	0.21
6	1.68	9.96	0.99	0.93
7	7.18	20.47	0.74	0.24
8	5.44	6.66	0.16	−0.32
9	4.42	6.65	−0.60	−0.25
10	2.86	6.47	0.67	0.12
11	2.43	7.46	0.89	0.66
12	5.28	14.58	0.88	0.75
13	6.50	15.57	0.42	0.23
14	7.97	8.25	0.72	0.51
15	1.46	3.58	0.94	0.44
16	2.18	9.10	0.93	0.65
17	2.14	5.33	0.98	0.85
18	6.11	9.81	0.93	0.68
19	7.15	7.10	0.68	0.76
20	5.92	6.30	0.78	0.56
Average	4.31	8.74	0.73	0.45

5. Conclusions and recommendations

Reliable estimates of precipitation are essential for hydrologic applications and water resources planning, since uncertainties of precipitation as a major input data can propagate into hydrological and meteorological models. Furthermore, detailed information of rainfall and a better understanding of its spatial and temporal distributions are importantly needed for predicting the available water resources and optimal planning to use them effectively. In fact, precipitation is a key component of the global hydrological cycle; also, understanding the underlying processes in the hydrological cycle is fundamental to water resources management and climate studies. Therefore, satellite-based precipitation-estimate techniques which provide extended precipitation coverage beyond ground in situ data are increasingly applied to atmospheric and hydrological applications at different space-time scales (Hong et al., 2006a,b). Nevertheless, satellite-retrieved precipitations are less direct than ground-based data and lead to uncertainty in estimates.

In this study, the uncertainties associated with two high resolution satellite precipitation products (PERSIANN and TMPA-3B42) were described and adjusted through copula-based model. Since it is well known that rainfall data are dependent in both space and time, similar spatial structure between generations and observation fields can be an important feature of rainfall simulation models. Therefore, a copula-based model that preserves the spatial dependency among variables independent of their marginal would be a useful method in the simulation of multivariate random fields. Here, a multivariate Gaussian copula was developed in order to simulate ensembles of bias-adjusted rainfall realizations of SREs. In order to measure the robustness of the simulated realizations of BASREs, two factors (P and R) were computed for each simulated ensemble by comparing it with the observed data. In fact, using P and R, one can predict the uncertainty associated with the BASREs quantitatively. Furthermore, since each set of randomly generated biases resulted in an individual pair of P and R factors for simulated ensemble, several sets of bias fields were generated randomly, a more appropriate set then was selected based on a better pairs of P and R values. This procedure can lead to a more accurate simulation of ensembles. With respect to the three statistical indices (*Bias*, *RMSE*, and *CC*) employed to evaluate the performance of the bias-adjusted realizations, one can argue that the developed model was able to improve the satellite rainfall estimates considerably. In addition, the validation results implied that the bias-adjusted band of the simulated realizations encompassed the observed data reasonably.

It is worth remembering that the uncertainty analysis framework presented here was based on the simulated ensembles of bias fields. In future research, it would be interesting to see how the technique reproduces the full distribution of bias using additional measures of reliability of the simulated ensembles. Various methods for the evaluation of ensemble-based forecasts can be found in the review by Toth et al. (2003). Moreover, using ensemble analysis instead of a

Table 4
Results of *Bias* of the six tested events over each pixel, comparison between the OSRE and BASRE (the 50% quantile of simulated realizations) for PERSIANN product.

Bias of tested events (PERSIANN)												
	Event 1		Event 2		Event 3		Event 4		Event 5		Event 6	
Pixel no	*Bias* (OSRE)	*Bias* (BASRE)	*Bias* (OSRE)	*Bias* (BASRE)	*Bias* (OSRE)	*Bias* (BASRE)	*Bias* (OSRE)	*Bias* (BASRE)	*Bias* (OSRE)	*Bias* (BASRE)	*Bias* (OSRE)	*Bias* (BASRE)
1	13.4	2.5	−3.3	−1.5	−5.8	−1.5	−8.4	−9.9	25.6	14.5	−16.1	−2.7
2	7.3	−6.3	12.7	12.2	13.8	16.2	6.2	−1.6	16.0	−2.0	−12.2	−2.4
3	10.0	−1.8	−0.4	3.0	−3.1	1.4	7.1	2.5	17.0	3.2	−13.2	0.0
4	7.9	−1.5	−3.6	0.6	−7.4	−2.8	1.9	−1.3	13.2	3.0	−9.9	1.0
5	8.0	0.0	−6.7	−2.5	−4.5	0.8	−0.3	−1.5	12.3	1.2	−15.9	−0.9
6	8.2	3.0	−7.2	−2.3	−7.7	0.0	2.7	−1.9	21.9	11.8	−14.5	−0.6
7	3.5	−0.5	−6.6	−2.5	−17.6	−8.5	8.1	2.3	24.3	12.0	−15.8	−2.0
8	10.6	3.8	−5.0	−0.5	−7.5	−1.2	3.7	1.1	1.7	−8.2	−6.7	2.9
9	3.1	−2.1	−6.2	2.0	−5.3	2.1	5.4	2.2	1.8	−7.3	−10.2	2.3
10	4.9	2.0	−7.8	−1.6	−7.2	0.4	4.3	1.7	5.3	−3.6	−11.5	0.6
11	4.0	0.7	0.8	4.4	−11.6	−2.3	4.0	1.5	17.5	8.9	−8.4	2.9
12	4.5	6.8	−1.3	1.3	−8.2	0.2	6.5	−6.7	11.1	−6.0	−16.5	−6.1
13	3.0	−3.0	2.9	4.5	−8.7	−1.3	21.4	15.6	17.5	2.3	−12.2	−1.2
14	2.7	10.3	4.9	9.4	−7.9	4.5	5.4	0.8	11.5	−3.7	−10.3	−1.7
15	1.5	−0.3	−3.0	0.4	−8.3	−0.7	1.3	−2.8	10.0	−0.3	−14.3	−1.8
16	1.1	−0.9	0.6	2.2	−2.3	5.5	4.0	−0.8	13.0	3.7	−14.0	−1.3
17	−2.5	−8.6	−0.9	−0.5	−6.2	1.8	2.4	−2.0	31.8	16.6	0.4	4.2
18	7.0	−1.5	4.0	2.6	−8.7	−5.0	7.0	1.7	38.8	24.3	1.5	2.4
19	−4.0	−4.5	3.5	3.8	−11.2	−2.6	7.2	3.0	25.5	15.7	−7.2	−0.3
20	2.4	5.0	3.1	3.2	−5.6	2.4	7.4	−1.8	12.8	−5.0	1.9	−10.8
Average	4.8	0.2	−1.0	1.9	−6.6	0.5	4.9	0.1	16.4	4.1	−10.2	−0.8

single realization, one can improve the uncertainty assessment of the error propagation from the precipitation input into the hydrological models and water resources simulations. Also, with respect to the extreme precipitation events, i.e., floods and droughts, using ensemble-based models, one can evaluate extreme prediction uncertainty and its associated risks for a specified precipitation.

In this study as a first attempt to quantify and adjust the uncertainty associated with two major satellite-based precipitation products over a developing region in Iran, a simple

Table 5
Results of *Bias* of the six tested events over each pixel, comparison between the OSRE and BASRE (the 50% quantile of simulated realizations) for TMPA-3B42 product.

Bias of tested events (TMPA-3B42)												
	Event 1		Event 2		Event 3		Event 4		Event 5		Event 6	
Pixel no	Bias (OSRE)	Bias (BASRE)	Bias (OSRE)	Bias (BASRE)	Bias (OSRE)	Bias (BASRE)	Bias (OSRE)	Bias (BASRE)	Bias (OSRE)	Bias (BASRE)	Bias (OSRE)	Bias (BASRE)
1	−6.6	−0.5	0.4	0.2	−0.6	1.0	−9.9	−6.5	16.4	12.9	−12.0	−0.4
2	11.9	−0.2	−20.3	−7.7	−10.1	−2.9	5.8	−1.0	12.8	0.0	5.9	6.3
3	4.6	−1.5	1.9	5.9	−2.0	0.8	−1.4	3.5	11.4	2.2	−7.2	1.4
4	9.4	−0.2	1.5	0.1	2.7	−3.8	−0.8	−2.0	13.7	−1.0	−10.7	−0.9
5	7.8	−1.2	−2.4	−1.9	−9.4	−2.0	2.0	−2.1	11.8	−1.8	−6.5	−0.9
6	−13.5	−2.0	−7.3	−1.9	−15.4	−1.3	0.3	−2.1	−10.7	−2.5	−2.5	2.1
7	−1.7	−3.5	−35.1	−7.2	−32.3	−13.0	−0.8	0.1	8.6	−0.3	−2.0	−0.1
8	13.9	3.0	0.1	−1.9	4.8	−1.4	3.5	−0.8	1.6	−12.8	5.9	0.9
9	7.3	−1.9	3.7	2.7	7.8	1.6	6.4	3.1	2.0	−11.9	−9.6	−0.1
10	8.2	0.4	−12.1	−2.0	4.1	−0.5	5.0	0.8	5.0	−8.8	−5.9	−1.4
11	−0.2	−2.5	−15.0	0.8	−7.8	−5.1	2.4	−0.4	18.9	3.5	−2.0	2.3
12	−23.8	5.1	−6.1	6.0	−21.2	6.3	5.2	7.5	−13.5	3.4	−3.7	1.5
13	−5.6	−5.0	−3.7	5.0	−26.4	−3.6	13.6	14.5	13.4	−0.8	3.9	−0.9
14	−7.2	6.5	−3.0	11.5	−14.4	9.2	2.2	9.0	11.2	4.0	3.3	5.1
15	5.9	1.0	−0.6	−0.4	2.8	0.0	−0.2	−2.6	10.2	−1.1	−5.9	−1.1
16	−7.8	−0.7	−0.7	0.6	−19.4	−0.7	3.5	−1.0	7.0	0.5	−0.6	0.0
17	3.2	−2.0	−1.2	0.0	−11.0	0.5	2.2	−0.8	4.9	3.3	3.1	0.9
18	4.4	−0.2	4.0	4.0	−11.3	−3.6	4.9	3.2	19.7	13.3	1.7	−0.8
19	3.0	−0.5	4.3	2.4	−1.0	1.2	7.4	3.4	24.4	15.7	−1.2	−1.9
20	0.7	1.8	1.8	7.0	−9.8	7.7	9.6	9.7	2.1	2.7	1.2	2.5
Average	0.7	−0.2	−4.5	1.2	−8.5	−0.5	3.0	1.8	8.5	1.0	−2.2	0.7

Table 6
Results of the P and R-factors of the six tested events for both PERSIANN and TMPA-3B42 products.

Satellite products	PERSIANN						TMPA-3B42					
Tested events	Event 1	Event 2	Event 3	Event 4	Event 5	Event 6	Event 1	Event 2	Event 3	Event 4	Event 5	Event 6
P-factor	65%	65%	80%	75%	50%	65%	80%	70%	80%	70%	70%	70%
R-factor	2.16	1.28	1.14	1.35	1.07	1.59	1.94	1.57	1.12	1.22	0.98	1.22

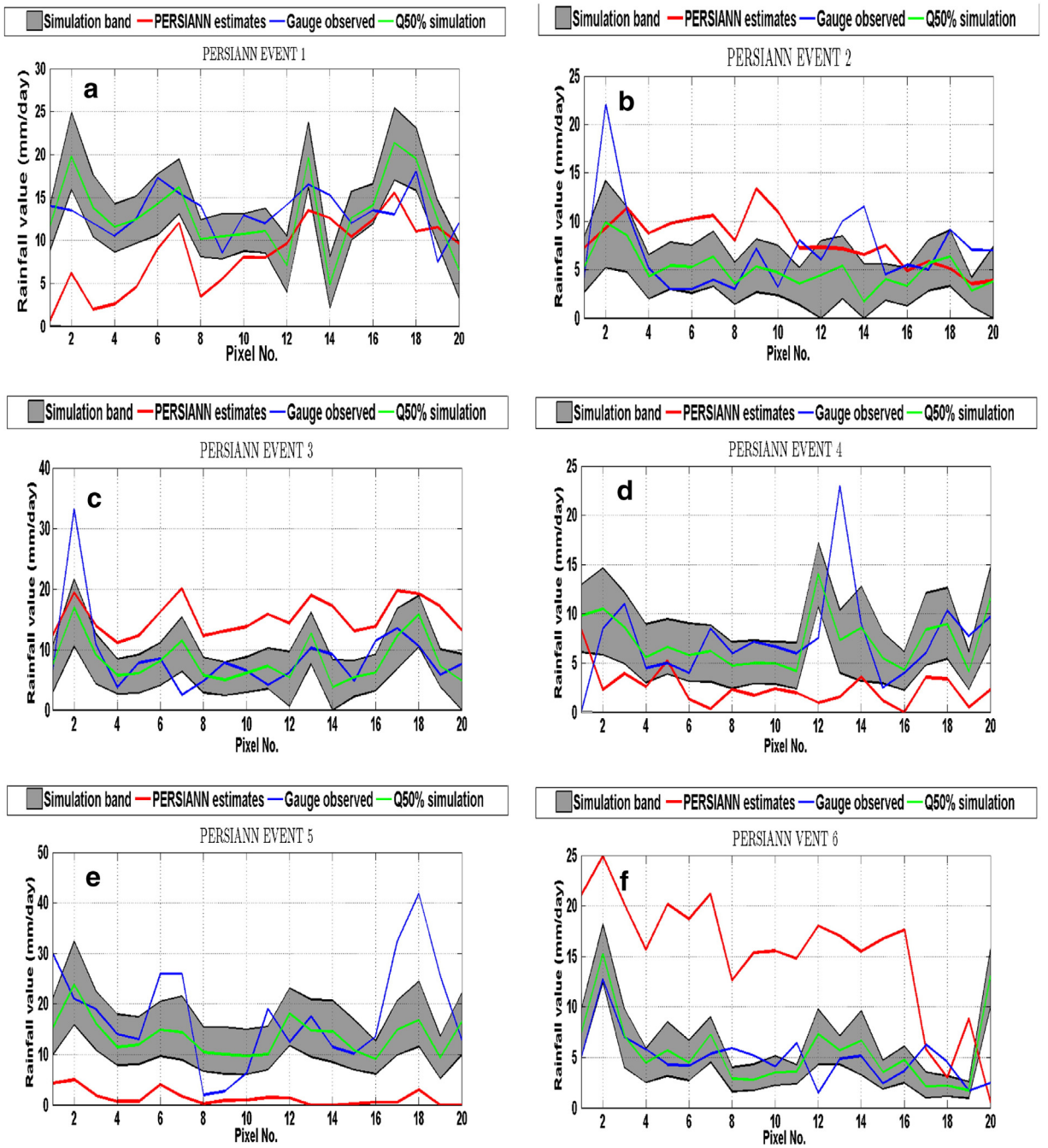

Fig. 10. Comparison between original PERSIANN rainfall estimates (red line), rain gauge observations (blue line), and 80% confidence band associated with bias-adjusted rainfall estimates (gray band) of the six tested daily events (a, b, c, d, e, f) over twenty studied pixels (vertical and horizontal axes represent the rainfall value (mm/day) and the number of pixel, respectively). (For interpretation of the references to color in this figure legend, the reader is referred to the web version of this article.)

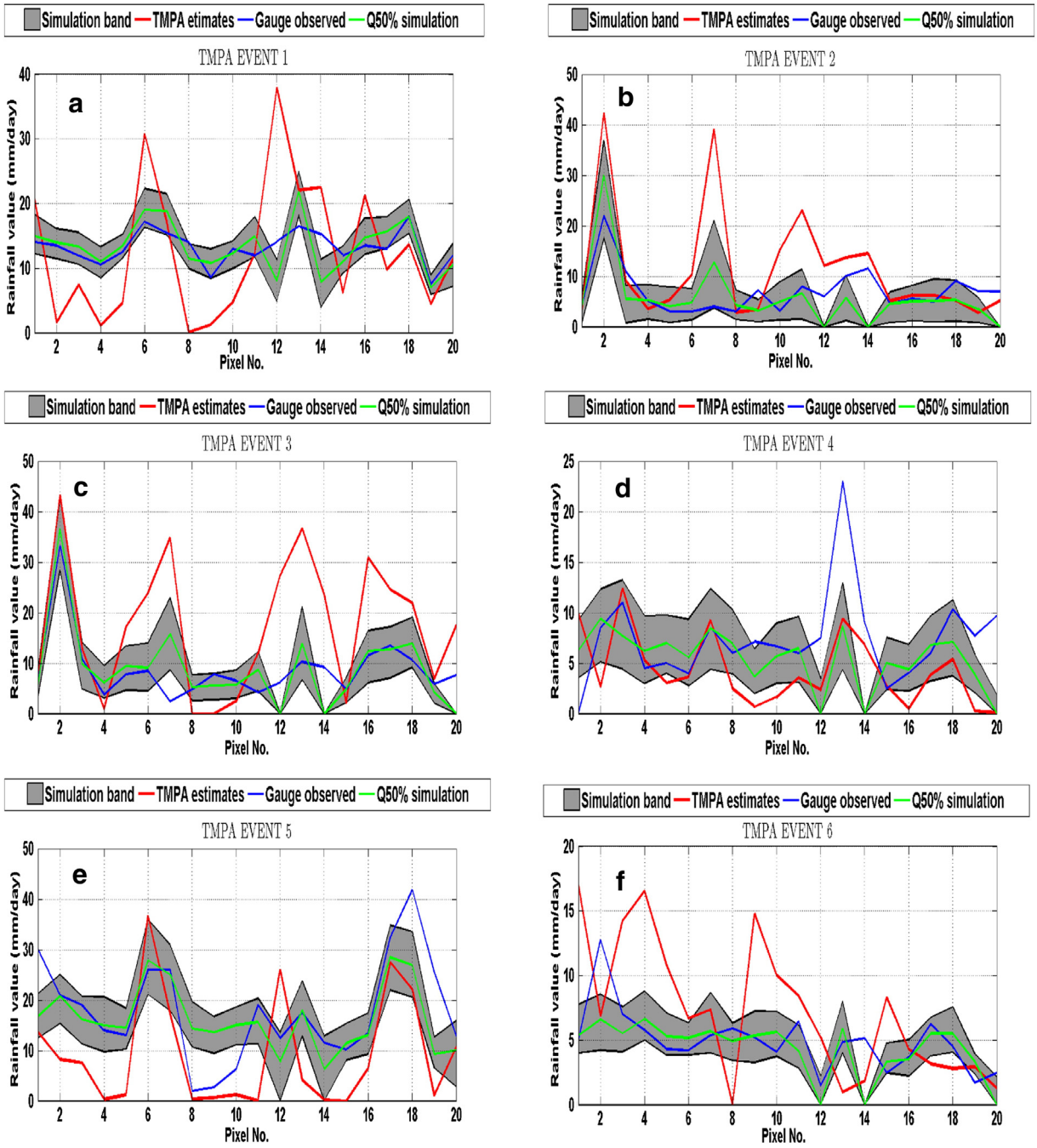

Fig. 11. Comparison between original TMPA-3B42 rainfall estimates (red line), rain gauge observations (blue line), and 80% confidence band associated with bias-adjusted rainfall estimates (gray band) of the six tested daily events (a, b, c, d, e, f) over twenty studied pixels (vertical and horizontal axes represent the rainfall value (mm/day) and the number of pixel, respectively). (For interpretation of the references to color in this figure legend, the reader is referred to the web version of this article.)

copula (Gaussian) was selected to simulations. However, for future research, one can implement the method presented here using t-copula as another elliptical copula.

The model proposed here was subject to various limitations such as unevenly distributed rain gauges over the study area. Indeed, 50% of the selected pixels contained one rain gauge that may be inadequate to have an accurate simulation. However, to alleviate the effect of gauge uncertainties, pixels with a minimum of three rain gauges are required (Habib et al., 2009). Additionally, unreliable surface gauge measurements

would result in erroneous parameter estimation, and consequently unrealistic ensembles of uncertainty fields. Therefore, to verify the appropriateness of the presented model, further investigations including simulations over regions with a dense rain gauge network, as well as in a fine temporal resolution (e.g. sub-daily) are required. Also, the presented approach in this paper cannot be applied directly to ungauged pixels without ground truth. In this case, the bias (observed or generated) could be extrapolated over ungauged pixels using geostatistical techniques, e.g. Inverse Distance Weighted (IDW) and Kriging (Shrestha, 2011).

Overall, the obtained results of this study indicated that the presented framework was able to adjust the uncertainty associated with the satellite precipitation products considerably. Moreover, the simulated biases and uncertainty bands here can be generalized over the ungauged basins where suffer from a lack of ground-based rainfall measurements considering the similarities in topography, physiography and climate conditions.

Acknowledgments

The authors would like to thank the two anonymous reviewers whose comments helped to improve the presentation significantly.

Appendix A. Probability distribution function of SREs bias

The fitted probability distribution function of fifty-four observed biases at each pixel is shown for PERSIANN and TMPA-3B42 products, respectively in Tables A1 and A2. Also, the related values of parameters for each marginal distribution are presented in these tables. Note that "GEV" in Tables A1 and A2 refers to Generalized Extreme Value distribution. The GEV distribution is a flexible three-parameter model that combines the Gumbel, Fréchet, and Weibull maximum extreme value distributions. It has the following PDF:

$$fx = \begin{cases} \frac{1}{\sigma}\exp\left(-(1+kz)^{-1/k}\right)(1+kz)^{-1-1/k} & k\neq \\ \frac{1}{\sigma}\exp(-z-\exp(-z)) & k=0 \end{cases} \quad \text{(A1)}$$

Where $z=(x-\mu)/\sigma$, x is the variable (here the value of bias), and k, σ, μ are the shape, scale, and location parameters respectively. The scale must be positive (sigma > 0), the shape and location can take on any real value. The range of definition of the GEV distribution depends on k:

$$\begin{array}{ll} 1+k\frac{(x-\mu)}{\sigma}>0 & \text{for} \quad k\neq 0 \\ -\infty < x < +\infty & \text{for} \quad k=0 \end{array} \quad \text{(A2)}$$

Various values of the shape parameter yield the extreme value type I, II, and III distributions. Specifically, the three cases $k=0$, $k>0$, and $k<0$ correspond, respectively, to the Gumbel, Fréchet, and Weibull families (Kotz and Nadarajah, 2000).

Table A1
Parametric distributions at each pixel for PERSIANN product.

Pixel no	Distribution	Parameter values		
1	GEV	$k=-0.098$	$\sigma=14.83$	$\mu=1.9$
2	GEV	0.06	21.7	11.16
3	Logistic		11.46	12.81
4	Normal		19.9	8.17
5	GEV	−0.027	14.01	−0.31
6	GEV	0.14	14.87	−0.577
7	GEV	0.145	16.03	1.34
8	Normal		16.24	5.92
9	Logistic		8.85	5.41
10	GEV	0.09	11.27	−1.029
11	Logistic		13.1	8.1
12	GEV	0.084	13.5	−0.247
13	Normal		22.98	14.75
14	Normal		22.97	17.91
15	GEV	0.184	11.44	−3.04
16	Logistic		7.72	5.07
17	GEV	0.176	15.75	3.183
18	Normal		25.44	19.4
19	Normal		15.33	3.91
20	GEV	0.243	12.32	−1.43

Appendix B. Correlation coefficient of SREs bias

In this section the CC values of SREs bias between each pair of twenty pixels are presented for both PERSIANN and TMPA-3B42 products, respectively in Tables B1 and B2. In these tables, "Obs", "Gen", and "Tes", respectively, refer to the fifty-four observed, one thousand generated, and six tested events. As shown the randomly generated biases retain the correlation imposed in the copula model which was derived from the observed values.

Table A2
Parametric distributions at each pixel for TMPA-3B42 product.

Pixel no	Distribution	Parameter values		
1	GEV	$k=-0.59$	$\sigma=23.9$	$\mu=-4.46$
2	Normal		23	16.5
3	GEV	−0.53	27.4	−4.43
4	Normal		30.03	−1.02
5	GEV	−0.7	26.7	−3.15
6	GEV	−0.4	32.16	−11.26
7	GEV	−0.65	37.3	−9.04
8	GEV	−0.71	26.9	−4.1
9	GEV	−0.45	19.8	−3.08
10	Logistic		13.87	1.06
11	GEV	−0.42	28.02	−8.5
12	Logistic		12.46	−0.116
13	Logistic		18.99	−0.805
14	GEV	−0.65	31.6	−0.66
15	GEV	−0.31	18.3	−4.91
16	Normal		23.74	−1.96
17	Logistic		15.37	4.74
18	GEV	−0.28	22.2	2.6
19	GEV	−0.14	14.6	−2.8
20	Normal		27.14	1.72

Table B1
The *CC* values of the bias between each pair of twenty pixels for PERSIANN product based on the fifty-four observed (Obs), one thousand generated (Gen), and six tested (Tes) events.

Event	Pixel	1	2	3	4	5	6	7	8	9	10	11	12	13	14	15	16	17	18	19	20
Obs	1	1.00	0.76	0.85	0.80	0.86	0.77	0.69	0.77	0.77	0.79	0.71	0.79	0.72	0.60	0.76	0.82	0.52	0.55	0.52	0.48
Gen		1.00	0.75	0.87	0.85	0.88	0.83	0.68	0.78	0.77	0.82	0.78	0.82	0.71	0.63	0.79	0.82	0.59	0.55	0.65	0.57
Tes		1.00	0.83	0.90	0.92	0.93	0.87	0.75	0.66	0.69	0.78	0.84	0.82	0.33	0.76	0.82	0.64	0.74	0.79	0.81	0.57
Obs	2	0.76	1.00	0.82	0.75	0.76	0.65	0.70	0.68	0.69	0.65	0.64	0.72	0.78	0.73	0.64	0.71	0.64	0.62	0.43	0.58
Gen		0.75	1.00	0.78	0.70	0.71	0.68	0.63	0.62	0.61	0.64	0.62	0.70	0.76	0.77	0.63	0.68	0.70	0.59	0.49	0.64
Tes		0.83	1.00	0.90	0.83	0.84	0.74	0.67	0.70	0.80	0.83	0.81	0.83	0.62	0.79	0.91	0.88	0.63	0.64	0.78	0.66
Obs	3	0.85	0.82	1.00	0.92	0.93	0.79	0.73	0.79	0.85	0.84	0.77	0.86	0.80	0.66	0.84	0.76	0.59	0.68	0.57	0.65
Gen		0.87	0.78	1.00	0.93	0.94	0.86	0.76	0.82	0.85	0.87	0.85	0.89	0.82	0.73	0.88	0.80	0.72	0.70	0.71	0.71
Tes		0.90	0.90	1.00	0.95	0.97	0.90	0.83	0.86	0.92	0.97	0.87	0.92	0.65	0.81	0.95	0.83	0.74	0.75	0.85	0.71
Obs	4	0.80	0.75	0.92	1.00	0.92	0.88	0.74	0.87	0.91	0.92	0.90	0.93	0.83	0.61	0.89	0.79	0.56	0.70	0.62	0.67
Gen		0.85	0.70	0.93	1.00	0.95	0.89	0.74	0.87	0.91	0.93	0.92	0.92	0.79	0.67	0.91	0.81	0.66	0.67	0.75	0.69
Tes		0.92	0.83	0.95	1.00	1.00	0.95	0.88	0.72	0.83	0.89	0.91	0.94	0.63	0.85	0.92	0.81	0.66	0.76	0.84	0.63
Obs	5	0.86	0.76	0.93	0.92	1.00	0.83	0.71	0.85	0.90	0.91	0.81	0.88	0.77	0.61	0.85	0.79	0.58	0.66	0.60	0.66
Gen		0.88	0.71	0.94	0.95	1.00	0.89	0.75	0.87	0.91	0.94	0.90	0.91	0.77	0.66	0.90	0.81	0.67	0.66	0.74	0.70
Tes		0.93	0.84	0.97	1.00	1.00	0.93	0.85	0.78	0.86	0.91	0.88	0.92	0.60	0.81	0.91	0.79	0.66	0.73	0.81	0.60
Obs	6	0.77	0.65	0.79	0.88	0.83	1.00	0.72	0.87	0.82	0.90	0.93	0.96	0.80	0.53	0.81	0.80	0.55	0.62	0.60	0.52
Gen		0.83	0.68	0.86	0.89	0.89	1.00	0.82	0.89	0.85	0.91	0.92	0.97	0.78	0.65	0.85	0.80	0.71	0.66	0.75	0.70
Tes		0.87	0.74	0.90	0.95	0.93	1.00	0.97	0.61	0.72	0.83	0.97	0.97	0.63	0.92	0.92	0.80	0.81	0.90	0.94	0.79
Obs	7	0.69	0.70	0.73	0.74	0.71	0.72	1.00	0.83	0.71	0.72	0.70	0.78	0.83	0.72	0.68	0.66	0.73	0.70	0.49	0.67
Gen		0.68	0.63	0.76	0.74	0.75	0.82	1.00	0.83	0.73	0.78	0.76	0.82	0.80	0.73	0.72	0.67	0.83	0.75	0.62	0.78
Tes		0.75	0.67	0.83	0.88	0.85	0.97	1.00	0.53	0.67	0.79	0.97	0.97	0.72	0.94	0.90	0.83	0.80	0.90	0.94	0.86
Obs	8	0.77	0.68	0.79	0.87	0.85	0.87	0.83	1.00	0.88	0.89	0.84	0.90	0.83	0.63	0.78	0.79	0.68	0.71	0.63	0.66
Gen		0.78	0.62	0.82	0.87	0.87	0.89	0.83	1.00	0.88	0.90	0.88	0.91	0.78	0.69	0.83	0.78	0.74	0.71	0.75	0.71
Tes		0.66	0.70	0.86	0.72	0.78	0.61	0.53	1.00	0.95	0.93	0.51	0.62	0.52	0.41	0.71	0.58	0.49	0.40	0.51	0.43
Obs	9	0.77	0.69	0.85	0.91	0.90	0.82	0.71	0.88	1.00	0.93	0.80	0.87	0.76	0.60	0.76	0.74	0.60	0.73	0.58	0.64
Gen		0.77	0.61	0.85	0.91	0.91	0.85	0.73	0.88	1.00	0.95	0.84	0.87	0.72	0.64	0.82	0.73	0.66	0.70	0.74	0.67
Tes		0.69	0.80	0.92	0.83	0.86	0.72	0.67	0.95	1.00	0.98	0.67	0.78	0.74	0.60	0.85	0.79	0.48	0.46	0.62	0.53
Obs	10	0.79	0.65	0.84	0.92	0.91	0.90	0.72	0.89	0.93	1.00	0.91	0.93	0.80	0.57	0.89	0.77	0.58	0.70	0.61	0.65
Gen		0.82	0.64	0.87	0.93	0.94	0.91	0.78	0.90	0.95	1.00	0.92	0.92	0.76	0.65	0.90	0.76	0.68	0.72	0.74	0.70
Tes		0.78	0.83	0.97	0.89	0.91	0.83	0.79	0.93	0.98	1.00	0.78	0.87	0.73	0.71	0.91	0.82	0.64	0.63	0.76	0.66
Obs	11	0.71	0.64	0.77	0.90	0.81	0.93	0.70	0.84	0.80	0.91	1.00	0.94	0.82	0.50	0.88	0.78	0.50	0.61	0.59	0.54
Gen		0.78	0.62	0.85	0.92	0.90	0.92	0.76	0.88	0.84	0.92	1.00	0.94	0.79	0.65	0.92	0.80	0.66	0.64	0.74	0.65
Tes		0.84	0.81	0.87	0.91	0.88	0.97	0.97	0.51	0.67	0.78	1.00	0.98	0.68	0.99	0.95	0.87	0.81	0.91	0.97	0.85
Obs	12	0.79	0.72	0.86	0.93	0.88	0.96	0.78	0.90	0.87	0.93	0.94	1.00	0.84	0.62	0.86	0.82	0.61	0.68	0.69	0.64
Gen		0.82	0.70	0.89	0.92	0.91	0.97	0.82	0.91	0.87	0.92	0.94	1.00	0.81	0.70	0.88	0.83	0.74	0.68	0.80	0.72
Tes		0.82	0.83	0.92	0.94	0.92	0.97	0.97	0.62	0.78	0.87	0.98	1.00	0.78	0.96	0.98	0.92	0.76	0.85	0.94	0.83
Obs	13	0.72	0.78	0.80	0.83	0.77	0.80	0.83	0.83	0.76	0.80	0.82	0.84	1.00	0.78	0.75	0.78	0.80	0.78	0.56	0.72
Gen		0.71	0.76	0.82	0.79	0.77	0.78	0.80	0.78	0.72	0.76	0.79	0.81	1.00	0.85	0.79	0.75	0.88	0.77	0.65	0.81
Tes		0.33	0.62	0.65	0.63	0.60	0.63	0.72	0.52	0.74	0.73	0.68	0.78	1.00	0.71	0.80	0.90	0.34	0.42	0.61	0.65
Obs	14	0.60	0.73	0.66	0.61	0.61	0.53	0.72	0.63	0.60	0.57	0.50	0.62	0.78	1.00	0.55	0.63	0.82	0.75	0.44	0.64
Gen		0.63	0.77	0.73	0.67	0.66	0.65	0.73	0.69	0.64	0.65	0.65	0.70	0.85	1.00	0.65	0.66	0.87	0.80	0.53	0.71
Tes		0.76	0.79	0.81	0.85	0.81	0.92	0.94	0.41	0.60	0.71	0.99	0.96	0.71	1.00	0.93	0.90	0.76	0.88	0.95	0.85
Obs	15	0.76	0.64	0.84	0.89	0.85	0.81	0.68	0.78	0.76	0.89	0.88	0.86	0.75	0.55	1.00	0.74	0.49	0.60	0.63	0.66
Gen		0.79	0.63	0.88	0.91	0.90	0.85	0.72	0.83	0.82	0.90	0.92	0.88	0.79	0.65	1.00	0.80	0.64	0.63	0.78	0.69
Tes		0.82	0.91	0.95	0.92	0.91	0.92	0.90	0.71	0.85	0.91	0.95	0.98	0.80	0.93	1.00	0.95	0.74	0.79	0.92	0.82
Obs	16	0.82	0.71	0.76	0.79	0.79	0.80	0.66	0.79	0.74	0.77	0.78	0.82	0.78	0.63	0.74	1.00	0.65	0.58	0.62	0.50
Gen		0.82	0.68	0.80	0.81	0.81	0.80	0.67	0.78	0.73	0.76	0.80	0.83	0.75	0.66	0.80	1.00	0.69	0.55	0.75	0.62
Tes		0.64	0.88	0.83	0.81	0.79	0.80	0.83	0.58	0.79	0.82	0.87	0.92	0.90	0.90	0.95	1.00	0.57	0.65	0.82	0.77
Obs	17	0.52	0.64	0.59	0.56	0.58	0.55	0.73	0.68	0.60	0.58	0.50	0.61	0.80	0.82	0.49	0.65	1.00	0.87	0.51	0.81
Gen		0.59	0.70	0.72	0.66	0.67	0.71	0.83	0.74	0.66	0.68	0.66	0.74	0.88	0.87	0.64	0.69	1.00	0.87	0.59	0.88
Tes		0.74	0.63	0.74	0.66	0.66	0.81	0.80	0.49	0.48	0.64	0.81	0.76	0.34	0.76	0.74	0.57	1.00	0.96	0.92	0.90
Obs	18	0.55	0.62	0.68	0.70	0.66	0.62	0.70	0.71	0.73	0.70	0.61	0.68	0.78	0.75	0.60	0.58	0.87	1.00	0.49	0.81
Gen		0.55	0.59	0.70	0.67	0.66	0.66	0.75	0.71	0.70	0.72	0.64	0.68	0.77	0.80	0.63	0.55	0.87	1.00	0.50	0.78
Tes		0.79	0.64	0.75	0.76	0.73	0.90	0.90	0.40	0.46	0.63	0.91	0.85	0.42	0.88	0.79	0.65	0.96	1.00	0.97	0.90
Obs	19	0.52	0.43	0.57	0.62	0.60	0.60	0.49	0.63	0.58	0.61	0.59	0.69	0.56	0.44	0.63	0.62	0.51	0.49	1.00	0.50
Gen		0.65	0.49	0.71	0.75	0.74	0.75	0.62	0.75	0.74	0.74	0.74	0.80	0.65	0.53	0.78	0.75	0.59	0.50	1.00	0.57
Tes		0.81	0.78	0.85	0.84	0.81	0.94	0.94	0.51	0.62	0.76	0.97	0.94	0.61	0.95	0.92	0.82	0.92	0.97	1.00	0.93
Obs	20	0.48	0.58	0.65	0.67	0.66	0.52	0.67	0.66	0.64	0.65	0.54	0.64	0.72	0.64	0.66	0.50	0.81	0.81	0.50	1.00
Gen		0.57	0.64	0.71	0.69	0.70	0.70	0.78	0.71	0.67	0.70	0.65	0.72	0.81	0.71	0.69	0.62	0.88	0.78	0.57	1.00
Tes		0.57	0.66	0.71	0.63	0.60	0.79	0.86	0.43	0.53	0.66	0.85	0.83	0.65	0.85	0.82	0.77	0.90	0.90	0.93	1.00

References

Abbaspour, K.C., Johnson, C.A., Van Genuchten, M. Th., 2004. Estimating uncertain flow and transport parameters using a sequential uncertainty fitting procedure. Vadose Zone J. 3, 1340–1352.

Abbaspour, K.C., Yang, J., Maximov, I., Siber, R., Bogner, K., Mieleitner, J., Zobrist, J., Srinivasan, R., 2007. Spatiallydistributed modelling of hydrology and water quality in the pre-alpine/alpine Thur watershed using SWAT. J. Hydrol. 333, 413–430.

AghaKouchak, A., 2010. Simulation of Remotely Sensed Rainfall Fields Using Copulas. Institut für Wasserbau der Universität Stuttgart.

AghaKouchak, A., Nasrollahi, N., Habib, E., 2009. Accounting for uncertainties of the TRMM satellite estimates. J. Remote Sens. 1, 606–619. http://dx.doi.org/10.3390/rs1030606.

Table B2
The *CC* values of the bias between each pair of twenty pixels for TMPA-3B42 product based on the fifty-four observed (Obs), one thousand generated (Gen), and six tested (Tes) events.

Event	Pixel	1	2	3	4	5	6	7	8	9	10	11	12	13	14	15	16	17	18	19	20
Obs	1	1.00	0.33	0.65	0.62	0.51	0.45	0.41	0.56	0.43	0.36	0.42	0.42	0.41	0.20	0.38	0.34	0.33	0.20	0.27	0.43
Gen		1.00	0.34	0.65	0.62	0.55	0.47	0.41	0.61	0.47	0.40	0.41	0.44	0.44	0.25	0.41	0.36	0.31	0.22	0.29	0.43
Tes		1.00	0.36	0.98	0.75	0.84	0.51	0.34	0.34	0.58	0.59	0.69	0.53	0.39	0.74	0.90	0.57	0.74	0.91	0.84	0.60
Obs	2	0.33	1.00	0.53	0.29	0.44	0.38	0.46	0.32	0.41	0.45	0.45	0.53	0.47	0.52	0.41	0.39	0.46	0.31	0.29	0.37
Gen		0.34	1.00	0.57	0.28	0.46	0.36	0.43	0.35	0.40	0.44	0.42	0.51	0.44	0.52	0.42	0.35	0.45	0.30	0.23	0.37
Tes		0.36	1.00	0.45	0.23	0.51	0.25	0.93	0.69	0.10	0.80	0.67	0.23	0.28	0.37	0.32	0.08	0.60	0.43	0.41	0.23
Obs	3	0.65	0.53	1.00	0.69	0.78	0.61	0.47	0.49	0.49	0.52	0.57	0.62	0.41	0.38	0.59	0.49	0.45	0.30	0.37	0.54
Gen		0.65	0.57	1.00	0.71	0.80	0.59	0.47	0.54	0.51	0.57	0.59	0.65	0.41	0.38	0.62	0.48	0.46	0.32	0.33	0.59
Tes		0.98	0.45	1.00	0.75	0.85	0.53	0.38	0.46	0.66	0.69	0.66	0.52	0.37	0.64	0.87	0.53	0.79	0.85	0.77	0.59
Obs	4	0.62	0.29	0.69	1.00	0.74	0.67	0.26	0.70	0.60	0.62	0.66	0.52	0.33	0.19	0.55	0.34	0.31	0.41	0.42	0.40
Gen		0.62	0.28	0.71	1.00	0.76	0.66	0.26	0.72	0.60	0.64	0.63	0.50	0.31	0.21	0.54	0.36	0.26	0.42	0.41	0.44
Tes		0.75	0.23	0.75	1.00	0.93	0.03	0.18	0.11	0.77	0.63	0.65	0.02	0.10	0.51	0.89	0.16	0.21	0.67	0.79	0.28
Obs	5	0.51	0.44	0.78	0.74	1.00	0.69	0.40	0.50	0.57	0.74	0.69	0.73	0.41	0.39	0.72	0.64	0.44	0.37	0.50	0.46
Gen		0.55	0.46	0.80	0.76	1.00	0.70	0.40	0.58	0.63	0.79	0.73	0.76	0.44	0.38	0.75	0.65	0.42	0.38	0.49	0.47
Tes		0.84	0.51	0.85	0.93	1.00	0.23	0.50	0.15	0.73	0.83	0.85	0.29	0.38	0.69	0.96	0.37	0.48	0.83	0.90	0.51
Obs	6	0.45	0.38	0.61	0.67	0.69	1.00	0.46	0.59	0.59	0.68	0.75	0.71	0.53	0.38	0.73	0.60	0.37	0.33	0.55	0.20
Gen		0.47	0.36	0.59	0.66	0.70	1.00	0.44	0.64	0.60	0.68	0.73	0.70	0.51	0.38	0.71	0.63	0.32	0.31	0.55	0.19
Tes		0.51	0.25	0.53	0.03	0.23	1.00	0.33	0.61	0.28	0.37	0.28	0.98	0.82	0.48	0.35	0.91	0.83	0.51	0.29	0.89
Obs	7	0.41	0.46	0.47	0.26	0.40	0.46	1.00	0.23	0.30	0.34	0.41	0.58	0.79	0.74	0.31	0.64	0.80	0.52	0.35	0.57
Gen		0.41	0.43	0.47	0.26	0.40	0.44	1.00	0.30	0.34	0.34	0.39	0.57	0.74	0.64	0.31	0.59	0.77	0.48	0.40	0.54
Tes		0.34	0.93	0.38	0.18	0.50	0.33	1.00	0.51	0.02	0.73	0.80	0.36	0.50	0.60	0.38	0.27	0.56	0.56	0.54	0.39
Obs	8	0.56	0.32	0.49	0.70	0.50	0.59	0.23	1.00	0.82	0.66	0.63	0.50	0.32	0.15	0.59	0.30	0.22	0.22	0.38	0.09
Gen		0.61	0.35	0.54	0.72	0.58	0.64	0.30	1.00	0.83	0.69	0.65	0.54	0.36	0.21	0.58	0.39	0.25	0.28	0.44	0.16
Tes		0.34	0.69	0.46	0.11	0.15	0.61	0.51	1.00	0.11	0.51	0.16	0.48	0.24	0.04	0.04	0.25	0.83	0.20	0.00	0.31
Obs	9	0.43	0.41	0.49	0.60	0.57	0.59	0.30	0.82	1.00	0.77	0.69	0.69	0.44	0.35	0.64	0.41	0.32	0.34	0.46	0.15
Gen		0.47	0.40	0.51	0.60	0.63	0.60	0.34	0.83	1.00	0.78	0.68	0.70	0.45	0.37	0.59	0.46	0.33	0.37	0.52	0.18
Tes		0.58	0.10	0.66	0.77	0.73	0.28	0.02	0.11	1.00	0.65	0.31	0.27	0.30	0.19	0.69	0.34	0.30	0.39	0.45	0.50
Obs	10	0.36	0.45	0.52	0.62	0.74	0.68	0.34	0.66	0.77	1.00	0.89	0.85	0.53	0.39	0.77	0.50	0.41	0.38	0.48	0.24
Gen		0.40	0.44	0.57	0.64	0.79	0.68	0.34	0.69	0.78	1.00	0.91	0.85	0.51	0.40	0.76	0.54	0.40	0.38	0.48	0.27
Tes		0.59	0.80	0.69	0.63	0.83	0.37	0.73	0.51	0.65	1.00	0.76	0.37	0.49	0.47	0.68	0.33	0.59	0.60	0.63	0.54
Obs	11	0.42	0.45	0.57	0.66	0.69	0.75	0.41	0.63	0.69	0.89	1.00	0.89	0.57	0.42	0.76	0.62	0.41	0.35	0.49	0.19
Gen		0.41	0.42	0.59	0.63	0.73	0.73	0.39	0.65	0.68	0.91	1.00	0.90	0.52	0.40	0.77	0.64	0.37	0.32	0.48	0.21
Tes		0.69	0.67	0.66	0.65	0.85	0.28	0.80	0.16	0.31	0.76	1.00	0.38	0.54	0.88	0.83	0.43	0.49	0.88	0.93	0.54
Obs	12	0.42	0.53	0.62	0.52	0.73	0.71	0.58	0.50	0.69	0.85	0.89	1.00	0.65	0.55	0.71	0.74	0.52	0.36	0.53	0.29
Gen		0.44	0.51	0.65	0.50	0.76	0.70	0.57	0.54	0.70	0.85	0.90	1.00	0.64	0.51	0.73	0.75	0.49	0.34	0.52	0.30
Tes		0.53	0.23	0.52	0.02	0.29	0.98	0.36	0.48	0.27	0.37	0.38	1.00	0.89	0.60	0.43	0.96	0.78	0.59	0.40	0.94
Obs	13	0.41	0.47	0.41	0.33	0.41	0.53	0.79	0.32	0.44	0.53	0.57	0.65	1.00	0.79	0.52	0.53	0.76	0.54	0.29	0.47
Gen		0.44	0.44	0.41	0.31	0.44	0.51	0.74	0.36	0.45	0.51	0.52	0.64	1.00	0.72	0.52	0.55	0.73	0.54	0.28	0.47
Tes		0.39	0.28	0.37	0.10	0.38	0.82	0.50	0.24	0.30	0.49	0.54	0.89	1.00	0.67	0.48	0.91	0.55	0.58	0.49	0.95
Obs	14	0.20	0.52	0.38	0.19	0.39	0.38	0.74	0.15	0.35	0.39	0.42	0.55	0.79	1.00	0.45	0.56	0.83	0.59	0.22	0.52
Gen		0.25	0.52	0.38	0.21	0.38	0.38	0.64	0.21	0.37	0.40	0.40	0.51	0.72	1.00	0.43	0.49	0.80	0.58	0.25	0.48
Tes		0.74	0.37	0.64	0.51	0.69	0.48	0.60	0.04	0.19	0.47	0.88	0.60	0.67	1.00	0.81	0.69	0.53	0.95	0.92	0.69
Obs	15	0.38	0.41	0.59	0.55	0.72	0.73	0.31	0.59	0.64	0.77	0.76	0.71	0.52	0.45	1.00	0.57	0.46	0.37	0.53	0.28
Gen		0.41	0.42	0.62	0.54	0.75	0.71	0.31	0.58	0.59	0.76	0.77	0.73	0.52	0.43	1.00	0.62	0.45	0.33	0.48	0.30
Tes		0.90	0.32	0.87	0.89	0.96	0.35	0.38	0.04	0.69	0.68	0.83	0.43	0.48	0.81	1.00	0.55	0.49	0.91	0.95	0.63
Obs	16	0.34	0.39	0.49	0.34	0.64	0.60	0.64	0.30	0.41	0.50	0.62	0.74	0.53	0.56	0.57	1.00	0.58	0.40	0.43	0.28
Gen		0.36	0.35	0.48	0.36	0.65	0.63	0.59	0.39	0.46	0.54	0.64	0.75	0.55	0.49	0.62	1.00	0.52	0.38	0.47	0.23
Tes		0.57	0.08	0.53	0.16	0.37	0.91	0.27	0.25	0.34	0.33	0.43	0.96	0.91	0.69	0.55	1.00	0.65	0.66	0.51	0.97
Obs	17	0.33	0.46	0.45	0.31	0.44	0.37	0.80	0.22	0.32	0.41	0.41	0.52	0.76	0.83	0.46	0.58	1.00	0.75	0.33	0.67
Gen		0.31	0.45	0.46	0.26	0.42	0.32	0.77	0.25	0.33	0.40	0.37	0.49	0.73	0.80	0.45	0.52	1.00	0.73	0.30	0.66
Tes		0.74	0.60	0.79	0.21	0.48	0.83	0.56	0.83	0.30	0.59	0.49	0.78	0.55	0.53	0.49	0.65	1.00	0.67	0.46	0.68
Obs	18	0.20	0.31	0.30	0.41	0.37	0.33	0.52	0.22	0.34	0.38	0.35	0.36	0.54	0.59	0.37	0.40	0.75	1.00	0.36	0.72
Gen		0.22	0.30	0.32	0.42	0.38	0.31	0.48	0.28	0.37	0.38	0.32	0.34	0.54	0.58	0.33	0.38	0.73	1.00	0.36	0.71
Tes		0.91	0.43	0.85	0.67	0.83	0.51	0.56	0.20	0.39	0.60	0.88	0.59	0.58	0.95	0.91	0.66	0.67	1.00	0.96	0.69
Obs	19	0.27	0.29	0.37	0.42	0.50	0.55	0.35	0.38	0.46	0.48	0.49	0.53	0.29	0.22	0.53	0.43	0.33	0.36	1.00	0.31
Gen		0.29	0.23	0.33	0.41	0.49	0.55	0.40	0.44	0.52	0.48	0.48	0.52	0.28	0.25	0.48	0.47	0.30	0.36	1.00	0.29
Tes		0.84	0.41	0.77	0.79	0.90	0.29	0.54	0.00	0.45	0.63	0.93	0.40	0.49	0.92	0.95	0.51	0.46	0.96	1.00	0.57
Obs	20	0.43	0.37	0.54	0.40	0.46	0.20	0.57	0.09	0.15	0.24	0.19	0.29	0.47	0.52	0.28	0.28	0.67	0.72	0.31	1.00
Gen		0.43	0.37	0.59	0.44	0.47	0.19	0.54	0.16	0.18	0.27	0.21	0.30	0.47	0.48	0.30	0.23	0.66	0.71	0.29	1.00
Tes		0.60	0.23	0.59	0.28	0.51	0.89	0.39	0.31	0.50	0.54	0.54	0.94	0.95	0.69	0.63	0.97	0.68	0.69	0.57	1.00

Aghakouchak, A., Habib, E., Bárdossy, A., 2010a. A comparison of three remotely sensed rainfall ensemble generators. Atmos. Res. 02234, 13.

AghaKouchak, A., Bárdossy, A., Habib, E., 2010b. Conditional simulation of remotely sensed rainfall data using a non-Gaussian v-transformed copula. Adv. Water Resour. 33, 624–634.

AghaKouchak, A., Bárdossy, A., Habib, E., 2010c. Copula-based uncertainty modelling: application to multisensor precipitation estimates. Hydrol. Process. 24, 2111–2124. http://dx.doi.org/10.1002/hyp.7632.

AghaKouchak, A., Behrangi, A., Sorooshian, S., Hsu, K., Amitai, E., 2011. Evaluation of satellite-retrieved extreme precipitation rates across the central United States. J. Geophys. Res. 116, D02115. http://dx.doi.org/10.1029/2010JD014741.

AghaKouchak, A., Mehran, A., Norouzi, H., Behrangi, A., 2012. Systematic and random error components in satellite precipitation data sets. Geophys. Res. Lett. 39, L09406. http://dx.doi.org/10.1029/2012GL051592.

Behrangi, A., Khakbaz, B., JaW, T.C., AghaKouchak, A., Hsu, K., Sorooshian, S., 2011. Hydrologic evaluation of satellite precipitation products over a mid-size basin. J. Hydrol. 397, 225–237. http://dx.doi.org/10.1016/j.jhydrol.11.043.

Bellerby, T., Sun, J., 2005. Probabilistic and ensemble representations of the uncertainty in an IR/microwave satellite precipitation product. J. Hydrometeorol. 6, 1032–1044.

Ben-Gal, I., 2005. Outlier detection. In: Maimon, O., Rockach, L. (Eds.), Data Mining and Knowledge Discovery Handbook: A Complete Guide for Practitioners and Researchers. Kluwer Academic Publishers. ISBN: 0-387-24435-2.

Bitew, M.M., Gebremichael, M., 2011. Evaluation of satellite rainfall products through hydrologic simulation in a fully distributed hydrologic model. Water Resour. Res. 47, W06526. http://dx.doi.org/10.1029/WR009917.

Cherubini, U., Luciano, E., Vecchiato, W., 2004. Copula Methods in Finance. John Wiley & Sons Ltd., The Atrium, Southern Gate, Chichester,West Sussex PO19 8SQ, England0-470-86344-7.

Ciach, G.J., Krajewski, W.F., Villarini, G., 2007. Product-error-driven uncertainty model for probabilistic quantitative precipitation estimation with NEXRAD data. J. Hydrometeorol. 8, 1325–1347. http://dx.doi.org/10.1175/2007JHM814.1.

Di Baldassarre, G., Laio, F., Montanari, A., 2009. Design flood estimation using model selection criteria. Phys. Chem. Earth 34 (10–12), 606–611.

Dinku, T., Connor, S.J., Ceccato, P., 2010. Comparison of CMORPH and TRMM-3B42 over mountainous regions of Africa and South America. In: Gebremichael, M., Hossaim, F. (Eds.), Satellite Rainfall Applications for Surface Hydrology. Springer Science+Business Media B.V., pp. 193–204.

Draper, N.R., Smith, H., 1998. Applied Regression Analysis, 3rd edition. Wiley Series in Probability and Statistics (ISBN-13: 978-0471170822).

Ebert, E.E., Janowiak, J.E., Kidd, C., 2007. Comparison of near-real-time precipitation estimates from satellite observations and numerical models. Bull. Am. Meteorol. Soc. 88, 47–64. http://dx.doi.org/10.1175/BAMS-88-1-47.

Evin, G., Favre, A.C., 2008. A new rainfall model based on the Neyman–Scott process using cubic copulas. Water Resour. Res. 44, W03433. http://dx.doi.org/10.1029/2007WR006054.

Fang, Y., 2012. Extensions to Gaussian Copula Models (A dissertation submitted to Oregon State University in partial fulfillment of the requirements for the degree of Doctor of Philosophy).

Favre, A.C., El Adlouni, S., Perreault, L., Thie'monge, N., Bobe'e, B., 2004. Multivariate hydrological frequency analysis using copulas. Water Resour. Res. W01101. http://dx.doi.org/10.1029/2003WR002456.

Filzmoser, P., 2005. A multivariate outlier detection method. Technical report. Department of Statistics and Probability Theory, Vienna, AUSTRIA.

Frahm, G., Junker, M., Schmidt, R., 2005. Estimating the tail-dependence coefficient: properties and pitfalls. Insur. Math. Econ. 37, 80–100.

Gebremichael, M., Krajewski, W.F., Morrissey, M.L., Huffman, G.J., Adler, R.F., 2005. A detailed evaluation of GPCP one-degree daily rainfall estimates over the Mississippi River Basin. J. Appl. Meteorol. 44 (5), 665–681.

Genest, C., Favre, A.-C., 2007. Everything you always wanted to know about copula modeling but were afraid to ask. J. Hydrol. Eng. 12 (4), 347–368.

Germann, U., Berenguer, M., Sempere-Torres, D., Salvade, G., 2006. Ensemble radar precipitation — a new topic on the radar horizon. Proceeding of the 4th European Conference on Radar in Meteorology and Hydrology ERAD, Barcelona, 18–22 September 2006.

Grimaldi, S., Serinaldi, F., 2006. Asymmetric copula in multivariate flood frequency analysis. Adv. Water Resour. 29, 1155–1167.

Habib, E., Henschke, A., Adler, R., 2009. Evaluation of TMPA satellite-based research and real-time rainfall estimates during six tropical-related heavy rainfall events over Louisiana, USA. Atmos. Res. http://dx.doi.org/10.1016/j.atmosres.2009.06.015.

Hirpa, F.A., Gebremichael, M., Hopson, T., 2010. Evaluation of high resolution satellite precipitation products over very complex terrain in Ethiopia. J. Appl. Meteorol. Climatol. 49, 1044–1051. http://dx.doi.org/10.1175/JAMC2298.1.

Hodge, V.J., and Austin, J., 2004. A Survey of Outlier Detection Methodologies. Dept. of Computer Science, University of York, York, UK, Kluwer Academic Publishers.

Hong, Y., Adler, R., Huffman, G., 2006a. Evaluation of the potential of NASA multi-satellite precipitation analysis in global landslide hazard assessment. Geophys. Res. Lett. 33, L22402. http://dx.doi.org/10.1029/GL028010.

Hong, Y., Hsu, K., Moradkhani, H., Sorooshian, S., 2006b. Uncertainty quantification of satellite precipitation estimation and Monte Carlo assessment of the error propagation into hydrologic response. Water Resour. Res. 42, W08421. http://dx.doi.org/10.1029/WR004398.

Hong, Y., Gochis, D., Cheng, J., Hsu, K., Sorooshian, S., 2007. Evaluation of PERSIANN-CCS rainfall measurement using the NAME event rain gauge network. J. Hydrometeorol. 8 (3), 469–482. http://dx.doi.org/10.1175/JHM574.1.

Hossain, F., Anagnostou, E.N., 2006. A two-dimensional satellite rainfall error model. IEEE Trans. Geosci. Remote Sens. 44 (6), 1511 (June 2006).

Huffman, G.J., Adler, R.F., Bolvin, D.T., Nelkin, E.J., 2010. The TRMM multisatellite precipitation analysis (TMPA). In: Hossain, F., Gebremichael, M. (Eds.), Chapter in Satellite Applications for Surface Hydrology. Springer.

Jiang, S., Ren, L., Hong, Y., Yong, B., Yang, X., Yuan, F., Ma, M., 2012. Comprehensive evaluation of multi-satellite precipitation products with a dense rain gauge network and optimally merging their simulated hydrological flows using the Bayesian model averaging method. J. Hydrol. 452–453, 213–225.

Joe, H., 1997. Multivariate Models and Dependence Concepts. Chapman Hall, London.

Johnston, K., 2004. ArcGIS 9: Using ArcGIS Geostatistical Analyst. Esri Press.

Kotz, S., Nadarajah, S., 2000. Extreme Value Distributions: Theory and Applications. Imperial College Press, London.

Laio, F., 2004. Cramer–von Mises and Anderson-Darling goodness of fit tests for extreme value distributions with unknown parameters. Water Resour. Res. 40, W09308. http://dx.doi.org/10.1029/2004WR003204.

Laio, F., Di Baldassarre, G., Montanari, A., 2009. Model selection techniques for the frequency analysis of hydrological extremes. Water Resour. Res. 45, 7. http://dx.doi.org/10.1029/WR006666.

Li, L., Hong, Y., Wang, J., Adler, R.F., Policelli, F.S., Habib, S., Irwn, D., Korme, T., Okello, L., 2009. Evaluation of the real-time TRMMbased multi-satellite precipitation analysis for an operational flood prediction system in Nzoia Basin, Lake Victoria, Africa. Nat. Hazards 50, 109–123. http://dx.doi.org/10.1007/s11069-008-9324-5.

Madsen, L., 2009. Maximum likelihood estimation of regression parameters with spatially dependent discrete data. J. Agric. Biol. Environ. Stat. 14, 375–391.

Mathes, A., Friederichs, P., Hense, A., 2008. Towards a quality control of precipitation data. Meteorol. Z. 17 (6), 733–749.

Nelsen, R., 2006. An Introduction to Copulas (Springer Series in Statistics). Springer Verlag, New York.

Renard, B., Lang, M., 2007. Use of a Gaussian copula for multivariate extreme value analysis: some case studies in hydrology. Adv. Water Resour. 30, 897–912.

Roca, R., Chambon, P., Jobard, I., Kirstetter, P.E., Gosset, M., Bergès, J.C., 2010. Comparing satellite and surface rainfall products over West Africa at meteorologically relevant scales during the AMMA campaign using error estimates. J. Appl. Meteorol. Climatol. 49, 715–731. http://dx.doi.org/10.1175/2009JAMC2318.1.

Rudolf, B., 1993. Management and analysis of precipitation data on a routine basis. In: Sevruk, B., Lapin, M. (Eds.), Proceedings of International Symposium on Precipitation and Evaporation, vol. 1. InSlovak Hydrometeorology Institution, pp. 69–76.

Schmidt, R., 2005. Tail dependence. In: Cizek, P., Ha¨rdle, W., Weron, R. (Eds.), Statistical Tools in Finance and Insurance. Springer, New York.

Schmidt, R., Stadtmuller, U., 2006. Non-parametric estimation of tail dependence. Scand. J. Stat. 33, 307–335.

Schuol, J., Abbaspour, K.C., Yang, H., Srinivasan, R., Zehnder, A.G.B., 2008. Modeling blue and green water availability in Africa. Water Resour. Res. 44, W07406. http://dx.doi.org/10.1029/2007WR006609.

Serinaldi, F., 2009a. Copula-based mixed models for bivariate rainfall data: an empirical study in regression perspective. Stoch. Environ. Res. Risk Assess. 23, 677–693.

Serinaldi, F., 2009b. A multisite daily rainfall generator driven by bivariate copula-based mixed distributions. J. Geophys. Res. 114, D10103. http://dx.doi.org/10.1029/2008JD011258.

Shrestha, M.S., 2011. Bias-Adjustment of Satellite-Based Rainfall Estimates over the Central Himalayas of Nepal for Flood Prediction. A Dissertation for the Degree of Doctor of Engineering Department of Civil and Earth Resources Engineering, Kyoto University, Japan.

Sklar, A., 1959. Fonctions de R´epartition `a n Dimensions et Leurs Marges, vol. 8. Publications de l'Institut de Statistique de L'Universit'e de: Paris, pp. 229–231.

Song, P.X.-K., 2000. Multivariate dispersion models generated from Gaussian copula. Scand. J. Stat. 27, 305–320.

Song, P.X.-K., Li, M., Yuan, Y., 2009. Joint regression analysis of correlated data using Gaussian copulas. Biometrics 65, 60–68.

Sorooshian, S., Hsu, K., Gao, X., Gupta, H.V., Imam, B., Braithwaite, D., 2000. Evaluation of the PERSIANN system satellite-based estimates of tropical rainfall. Bull. Am. Meteorol. Soc. 81 (9), 2035–2046.

Su, F., Hong, Y., Lettenmaier, D.P., 2008. Evaluation of TRMM Multisatellite Precipitation Analysis (TMPA) and its utility in hydrologic prediction in the La Plata basin. J. Hydrometeorol. 9 (4), 622–640. http://dx.doi.org/10.1175/JHM944.1.

Teo, C.K., Grimes, D.I.F., 2007. Stochastic modelling of rainfall from satellite data. J. Hydrol. 346 (1–2), 33–50.

Tian, Y., Lidard-Peters, C.D., Choudhury, B.J., Garcia, M., 2007. Multitemporal analysis of TRMM-based satellite precipitation products for land data assimilation applications. J. Hydrometeorol. 8 (6), 1165–1183. http://dx.doi.org/10.1175/2007JHM859.1.

Tian, Y., Huffman, G.J., Adler, R.F., Tang, L., Sapiano, M., Maggioni, V., Wu, H., 2013. Modeling errors in daily precipitation measurements: additive or multiplicative? Geophys. Res. Lett. 2013.

Toth, Z., Talagrand, O., Candille, G., Zhu, Y., 2003. Probability and ensemble forecasts. In: Jolliffe, I.T., Stephenson, D.B. (Eds.), Forecast Verification. Wiley, Chichester, UK, pp. 137–164.

Vandenberghe, S., Verhoest, N.E.C., Baets, B.De., 2010. Fitting bivariate copulas to the dependence structure between storm characteristics: a detailed analysis based on 105 year 10 min rainfall. Water Resour. Res. 46, W01512. http://dx.doi.org/10.1029/2009WR007857.

Villarini, G., Krajewski, W.F., Ciach, J.G., Zimmerman, D.L., 2009. Product-error-driven generator of probable rainfall conditioned on WSR-88D precipitation estimates. Water Resour. Res. 45, W01404. http://dx.doi.org/10.1029/2008WR006946.

Wang, X., Gebremichael, M., Yan, J., 2010. Weighted likelihood copula modeling of extreme rainfall events in Connecticut. J. Hydrol. 390, 108–115.

Werner, M., 2003. Identification of multivariate outliers in large data sets. A thesis submitted to the University of Colorado at Denver in partial fulfillment of the requirements for the degree of Doctor of Philosophy Appl. Math 12–41.

Wilks, D.S., 2006. Statistical Methods in the Atmospheric Sciences, 2nd edition. Academic Press, Burlington, MA (627 pp.).

Yang, J., Reichert, P., Abbaspour, K.C., Xia, J., Yang, H., 2008. Comparing uncertainty analysis techniques for a SWAT application to the Chaohe Basin in China. J. Hydrol. 358, 1–23.

Yong, B., Hong, Y., Ren, L.L., Gourley, J.J., Huffman, G.J., Chen, X., Wang, W., Khan, S.I., 2012. Assessment of evolving TRMM-based multisatellite real-time precipitation estimation methods and their impacts on hydrologic prediction in a high latitude basin. J. Geophys. Res. 117, D09108. http://dx.doi.org/10.1029/2011JD017069.

You, J., Hubbard, K.G., Nadarajah, S., Kunkel, K.E., 2007. Performance of quality assurance procedures on daily precipitation. J. Atmos. Ocean. Technol. 24, 821–834.

Zhang, L., Singh, V.P., 2007. Bivariate rainfall frequency distributions using Archimedean copulas. J. Hydrol. 332, 93–109.